Observatoire de Paris-Meudon

ANALYSIS OF SUBSOLAR MASS BLACK HOLE CANDIDATES IN ADVANCED LIGO-VIRGO DATA

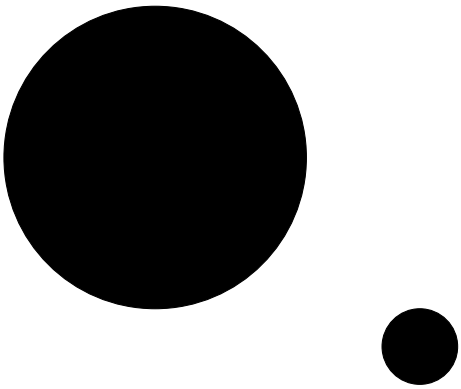

Author: Marine Prunier

Starting date of project: 05/03/2022 **Duration:** 4 months

Supervisor: Prof. Sébastien Clesse (Université Libre de Bruxelles)

Declaration of Authenticity

Je soussignée Marine Prunier certifie sur l'honneur :

— que les résultats décrits dans ce rapport sont l'aboutissement de mon travail

— que je suis l'auteure de ce rapport

— que je n'ai pas utilisé des sources ou résultats tiers sans clairement les citer et les référencer selon les règles bibliographiques préconisées.

Je déclare que ce travail ne peut être suspecté de plagiat.

Ce rapport de stage et le travail qui y est présenté sont les miens. À l'exception des Figures référencées 1, 2 et 14 dans la sous-section 1.2, j'ai produit tous les graphiques présentés dans ce rapport.

June 22, 2023 Signature:

Abstract

Gravitational wave astronomy has opened new windows for the detection of theoretical black holes of primordial origin. Primordial Black Holes may have formed from the collapse of overdense regions in the very early Universe. The detection of such objects would have ground-breaking implications for astrophysics and fundamental physics. Unlike stellar black holes, the cosmological origin of those primordial black holes does not prevent them from existing at subsolar masses. In 2022, a search for binary black hole mergers with at least one subsolar mass component was carried out by the LIGO-Virgo-KAGRA collaboration, with several candidates discovered. In this work, we aim to analyze one of the most promising of these candidates in order to infer the masses of the two compact objects that generated the gravitational wave signal. We perform a complete Bayesian parameter estimation on the candidate and find that the signal, if originating from a compact binary coalescence, has both components subsolar with $m_1 = 0.53^{+0.32}_{-0.11}$ and $m_2 = 0.29^{+0.07}_{-0.10}$ solar masses (1-sigma error bars). These masses are below the minimum mass of a neutron star, discarding the hypothesis that the signal is a binary neutron star. The significance of the candidate is also evaluated. The goal is to quantify the odds that the signal comes from a gravitational wave event rather than generated by noise in the detector. However, the various tests performed do not provide conclusive evidence to discriminate between either hypothesis.

Keywords: Primordial Black Holes, Gravitational Waves, Parameter Estimation.

Résumé

L'essor de l'astromie gravitationelle a ouvert de nouvelles perspectives pour la détection de trous noirs théoriques d'origine primordiale. Les trous noirs primordiaux se seraient formés à partir de l'effondrement gravitationnel de régions surdenses dans l'Univers très jeune. La détection de tels objets aurait des implications révolutionnaires pour l'astrophysique et la physique fondamentale. Contrairement aux trous noirs stellaires, l'origine cosmologique de ces trous noirs primordiaux n'empêche pas leur existence à des masses subsolaires dans l'Univers. En 2022, une recherche de fusions de trous noirs binaires ayant au moins une composante de masse subsolaire a été effectuée par la collaboration LIGO-Virgo-KAGRA, plusieurs candidats ont été découverts. Dans ce travail, nous cherchons à analyser l'un des candidats les plus prometteurs afin de déduire les masses des deux objets compacts qui ont générés ce signal. Nous effectuons une estimation complète des paramètres du signal gravitationnelle et trouvons que, si celui-ci provient bien d'une coalescence d'objet compact, il possède ces deux composants subsolaires avec $m_1 = 0.53^{+0.32}_{-0.11}$ et $m_2 = 0.29^{+0.07}_{-0.10}$ masses solaires. Ces masses sont inférieures à la masse minimale d'une étoile à neutron, ce qui permet de rejeter l'hypothèse que le signal provient d'une binaire d'étoile à neutron. La probabilité que le signal soit issu d'un événement d'onde gravitationnelle plutôt que généré par du bruit dans le détecteur est aussi analysée. Cependant, ces différents tests ne fournissent pas de preuves concluantes permettant de discriminer l'une des deux hypothèses.

Keywords: Trous Noirs Primordiaux, ondes gravitationnelles, estimation de paramètre.

Glossary

- BBH: Binary Black Hole
- BH: Black Hole
- BNS: Binary Neutron Star
- DM: Dark Matter
- FAR: False Alarm Rate
- FAP: False Alarm Probability
- GW: Gravitational Wave
- KAGRA: Kamioka Gravitational Wave Detector
- iFAR: inverse False Alarm Rate
- ISCO Innermost Stable Circular Orbit
- LIGO: Laser Interferometer Gravitational-Wave Observatory
- LVK: LIGO-Virgo-KAGRA collaboration
- MCMC: Monte Carlo Markov Chain
- NSBH: Binary Black Hole Neutron Star
- PBH: Primordial Black Hole
- PE: Parameter Estimation
- QCD: Quantum ChromoDynamic phase transition
- SMBH: SuperMassive Black Hole
- SNR: Signal to Noise Ratio
- SSM: SubSolar-Mass

Contents

1 Introduction and Overview

1.1 Motivation: hunt for subsolar-mass binary black holes

The very first detection of a gravitational wave event by the LIGO observatory in September 2015 [1] opened a whole new astronomy era; gravitational wave astronomy. Since then, the LIGO-Virgo-KAGRA (LVK) collaboration has reported nearly a hundred gravitational-wave (GW) events from the coalescence of compact binary systems [2]. LVK detectors are designed to jointly detect space-time deformations induced by the passage of gravitational waves produced by the merging of distant compact objects such as binary black holes or neutron stars.

The detection of the first binary black holes mergers revived the interest of the scientific community for theoretical compact objects of primordial origin: Primordial Black Holes (PBHs) [3] [4] [5]. PBHs may have formed in the early Universe, shortly after inflation ended, from the direct collapse of highly overdense regions. Such regions would result from large density fluctuations of the very early universe. When re-entering the Hubble horizon after the inflation, the density fluctuation - if above a critical density threshold - would have gravitationally collapsed to form a black hole. As the parameter space of dark matter particle models (such as the Weakly Interacting Massive Particule WIMP [6]) is becoming now tightly constrained, other non-particle candidates are attracting considerable attention. PBHs are considered good candidates to explain a fraction - or the totality - of the Dark Matter.

Gravitational wave astronomy opened a new window to the direct detection of PBHs, with great interest in the detection of subsolar-mass PBHs. Indeed, stellar evolution models predict that neither black holes nor neutron stars can be subsolar-mass compact objects. Therefore, detecting a subsolar-mass black hole would clearly sign a new formation mechanism alternative to this classic formation scenario. The discovery of a subsolar-mass black hole merger would be a smoking gun for a primordial origin and would lead to revolutionary implications in cosmology.

Several gravitational wave searches for binary systems having at least a component mass of less than 1 $M_\odot$ were carried out using the Advanced LIGO-Virgo data ([7] [8][9] [10][11] [12]) with no firm detection of subsolar-mass binary black holes. The most significant candidates do not have a sufficient low false-alarm rate (FAR; how often noise can produce an event similar to a real GW event) and high signal-to-noise ratio (SNR) to claim a discovery. However, these candidates are very promising and, as the sensitivity of the detectors is constantly being improved, the perspectives for the future detection of a subsolar black hole are positive.

In this work, we focus on the four candidates of subsolar-mass binary black hole events reported in the latest LIGO-Virgo observing run, O3b [2] (presented in Table 1). These signals are **not classified as confirmed subsolar-mass GW events** but rather as **candidates events** due to their SNR being just below, and FAR just above, the threshold to classify them as events. The hypothesis that these triggers are not of astrophysical origin is not yet ruled out. However, those candidates are raising the LIGO-Virgo-KAGRA interest, the collaboration published in February 2023 an article authored by all LIGO-Virgo members on the results of this extended search for subsolar-mass black hole binaries [13].

In this project, I further investigate these subsolar-mass candidates using GW's standard parameter estimation methods. I focus on the first candidate event reported in Table 1, SSMC1. It is the most significant candidate of the search, observed by both LIGO Hanford and LIGO Livingston detectors, both search methods (the GstLAL [14] and MBTA [15] pipelines) and

with a low false alarm probability. I analyze in detail the data and perform a careful parameter estimation of the signal. As a by-product, the parameter estimation allows to infer several physical characteristics of the candidate event (such as its component masses, spins, distance, and sky location). In particular, the probability of SSMC1 having subsolar-mass components can be inferred, if one assumes that the signal is coming from a true binary black hole event.

Table 1: Subsolar-mass black holes candidate events from the third observational run of the Advanced LIGO-Virgo [13]. m_1, m_2 corresponds to the masses of the GW template that best matches the detected signals. It is a rough estimate of the binary black hole masses and needs further investigation with a robust parameter estimation technique. In red is the candidate studied in this work. SSM170401 is a candidate from the O2 observing run (2019 [9]) analyzed in detail in [10].

Candidate	**FAR** [yr^{-1}]	**SNR**$_{tot}$	**Detector**	**Pipeline**	m_1 [$M_\odot$]	m_2 [$M_\odot$]
SSMC1	0.20	8.90	HL	GstLAL & MBTA	0.78	0.23
SSMC2	2.04	10.09	HLV	MBTA	1.24	0.53
SSMC3	1.56	9.10	HL	GstLAL & MBTA	1.52	0.27
SSMC4	1.37	10.25	HLV	MBTA	0.40	0.24
SSM170401	0.41	8.67	HL	GstLAL	4.89	0.77

Context of the project For this project, I worked under the supervision of Prof. Clesse, member of the Theoretical Physics group at Université Libre de Bruxelles and of the LVK collaboration. I have been added as a temporary member of the LIGO collaboration and have accessed many LIGO resources and computer services. I was included in the LVK Primordial Black Hole - Dark Matter (PBH-DM) group which focuses on the detection and analysis of subsolar-mass triggers. I participated in the group's weekly meetings and their discussions.

The group has conducted several searches for gravitational waves from subsolar-mass black hole binaries in the detectors' data and has performed the analysis of a candidate in the O2 run [10]. They are focusing as well on different topics around subsolar-mass binary black hole detections, from the efficiency of the search methods, the prediction and modelization of the characteristics of such events, to the analysis of candidates.

I was involved in two tasks within the group :

- **Main Task:** Perform a parameter estimation on two candidates events of Table 1. Find methods and tools to estimate the significance of events; quantify the probability that the signal is a real GW event and not a series of noises in the detector that would mimic a gravitational signal.
- **Sub Task:** Understand the differences between each GW search method (pipelines MBTA [15], GstLAL [14], and PyCBC [16]) and determine their respective efficiency for the search of subsolar-mass black holes.

I have not included in this report the work done on the second task as it mainly consisted of literature reviewing the pipelines search method and discussing with different LVK teams in charge of those pipelines. In Appendix A is linked the document summarising my work on studying the differences between search pipelines. This document is meant to be shared and updated with the PBH-DM group as a baseline to understand how the pipelines compute the SNR, FAR and rank a trigger to the status of GW event.

DISCLAIMER The goal of my work is not to claim the detection of subsolar-mass black holes by the Advanced LIGO-Virgo. The possibility that these candidates are not of astrophysical origin but induced by environmental or instrumental noise is yet not excluded. The parameter estimation and analysis aim to prepare for future O4 and O5 observing runs and subsequent subsolar-mass black hole searches. As the detectors have not yet reached their final design sensitivities and are improving in detecting weak GW signals, it is essential to have a robust set of tools to analyze future potential real subsolar triggers.

The purpose of the following two subsections is to provide a literature and state-of-the-art review on several aspects of primordial black hole theory and gravitational wave astronomy.

1.2 Primordial Black Holes as a dark matter candidate

Primordial Black Holes (PBHs) have been introduced more than 50 years ago by Zeldovich and Novikov in 1969 [17], and independently by Hawking in 1971 [18], as hypothetical black holes formed in the early Universe. The theory has recently been a source of intense interest among cosmologists even if there is still no definitive evidence for them.
PBHs are expected to be formed in the radiative era of the very early Universe through the collapses of high-density regions caused by large primordial density perturbations. These perturbations are characterized by a great amplitude, larger than a certain threshold δ_c, measured when the perturbations reenter the cosmological horizon.

Classical stellar black holes created from the collapse of a massive star can be characterized by an extremely dense amount of energy in a very compact region, i.e., the Schwarzschild radius, $R_s = \frac{2GM}{c^2}$, with mean density $\rho_s = \frac{M_{PBH}}{4\pi R_S^3} = 10^{18} \left(\frac{M}{M_\odot}\right)^{-2}$ g.cm^{-3}. On the other hand, PBHs are formed in the radiation era in the early Universe. With inflation, we have the creation of density fluctuations of different sizes causally disconnected -out of the Hubble horizon- which are therefore frozen and no longer evolving. With the expansion of the Universe and the size of the horizon increasing, these fluctuations will gradually re-enter the horizon. If at the time of re-entry into the Hubble horizon, the amplitude of the fluctuations exceeds a certain critical threshold δ_c, it collapses to create a Primordial Black Hole. The mass of this black hole corresponds roughly to the mass contained in the patch Hubble horizon M_H at the time of the collapse. The mean density of the universe during the radiation era scales with time as $\rho_c \sim 10^6 \left(\frac{t}{s}\right)^{-2}$ g.cm^{-3}. In order to have PBH formation, densities at least of the order of $\rho_c \sim \rho_s$ inside the black hole horizon are needed, which gives us:

$$M_{PBH} \sim M_H = \frac{c^3}{2GH} \sim 10^{15}\mathtt{g} \left(\frac{t}{10^{-23}\mathtt{s}}\right) \tag{1}$$

where H is the Hubble constant ($H = 67.8$ km/s from Planck15 [19]).

Using the above equation, we see that **PBHs with masses of ~ 1 $M_\odot$** would have been formed around one microsecond in the early universe, which corresponds to the Quantum Chromodynamics (QCD) phase transition (when the quark-gluon soup transitions to composite particles named hadrons). During this phase transition, the state equation of the Universe changes and the density threshold δ_c decreases leading to the boost of PBHs creation at ~ 1 $M_\odot$. Light PBHs with mass smaller than 10^{15} g are predicted to be evaporated through the Hawking radiation [20], implying that only the PBHs with larger masses can survive until today.

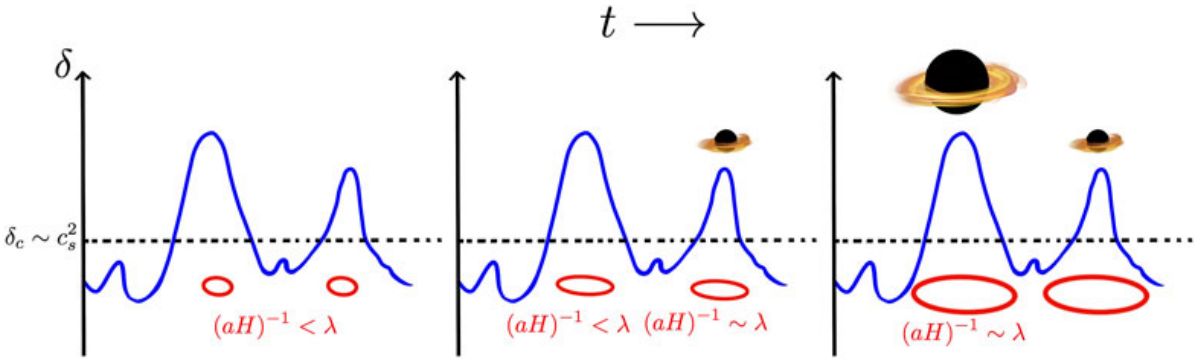

Figure 1: Sketch of the formation mechanism of PBHs from the collapse of high-density regions in the post-inflation Universe. In blue are the density fluctuations δ, and in red is the size of the Hubble horizon $(aH)^{-1}$. When a fluctuation with characteristic scale λ enters the Hubble Horizon at time t, the part of the density fluctuation above the critical threshold δ_c collapses and a PBH is produced. Fluctuations with larger λ enter the horizon later and lead to more massive PBHs. Figure taken from [21]

Motivation for dark matter-PBHs Primordial black holes' properties - nearly collisionless, stable, non-relativistic, and formed in the early ages of the Universe - make them a viable dark matter candidate. Like all the other dark matter candidates, PBHs have been theoretically and experimentally tested and many constraints on their abundance, assuming that they account for a part of the total dark matter mass, were obtained. For a complete and recent review see [22]. On the other hand, Figure 2 summarizes positive evidence for Primordial Black Holes (PBHs) in terms of the fraction f_{PBH} of the dark matter in PBHs with masses around M that could explain several astrophysical detections.

There is still no evidence that PBHs provide a part of the dark matter, but even if PBHs are not significantly contributing to the missing matter of the Universe, they could play an important cosmological role in seeding the cosmic structures and would provide a unique probe of the early Universe.

1.3 Gravitational wave detection and hunt for subsolar-mass binary black holes.

Gravitational waves are the space-time deformations generated when massive compact objects move with extreme accelerations (either Binary Neutron Stars (BNS), Binary Black Holes (BBH) or Neutron Star-Black Hole Binaries (NSBH)).
The typical life cycle of a BBH is the following. The two compact objects steadily lose their orbital binding energy by emission of GWs; as a result, the orbital separation between them decreases, and their orbital frequency increases. Their orbit keeps shrinking until the black holes coalesce into a singular BH while emitting a huge amount of gravitational waves. The frequency of this GW signal *chirps* in time, meaning that the signal becomes higher and higher pitched until the two objects collide and merge. This *chirp* can be observed in Fig.4 showing the GWs amplitude and frequency variation over time during the first detection of a binary neutron star in 2017. At the last stable orbit (Innermost Stable Circular Orbit ISCO), before the transition from the inspiral phase to the merger, the maximum frequency of the binary is reached [24]:

$$f_{ISCO} = \frac{1}{6^{3/2}\pi(m_1+m_2)} = 4.4\left(\frac{M_\odot}{m_1+m_2}\right)\text{kHz} \tag{2}$$

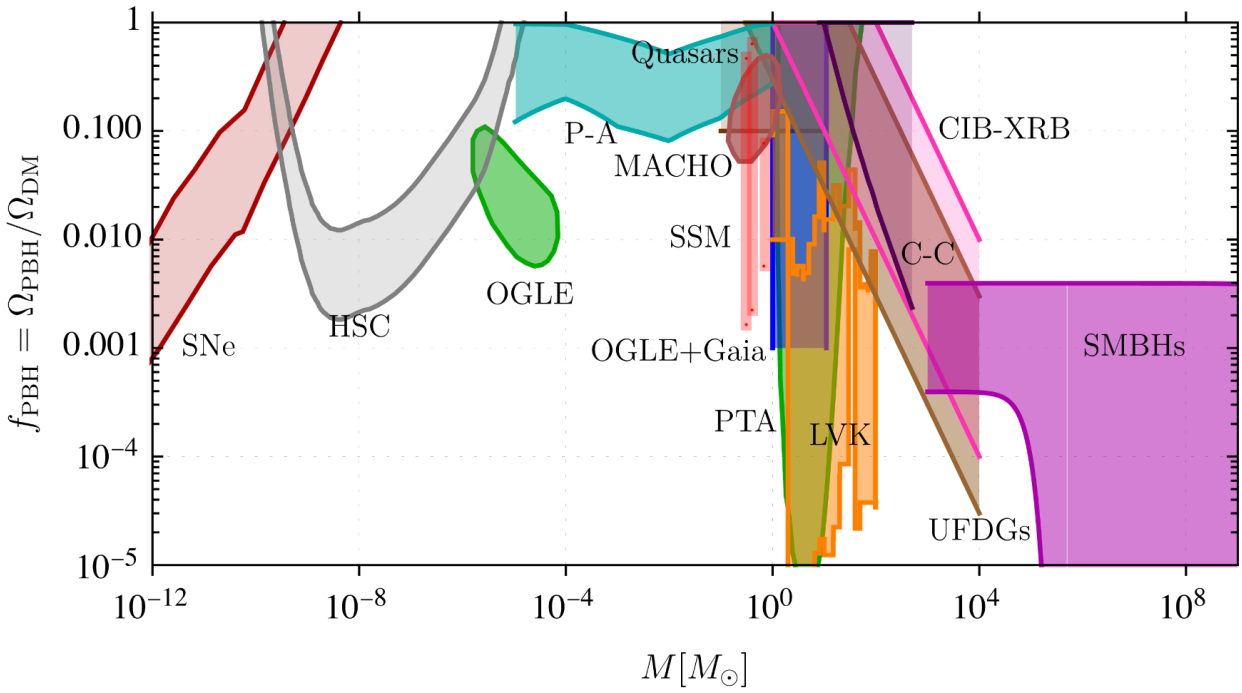

Figure 2: Summary of positive evidence for Primordial Black Holes (PBHs) (f_{PBH} is the fraction of Primordial Black Holes that could constitute dark matter). *How to read the graph:* for example, the detected microlensing effect if generated by PBHs of mass 10^{-5} $M_\odot$ could explain $\approx 1\%$ of the dark matter. These constraints come from PBH-attributed signals from supernovæ (SNe), various microlensing surveys, gravitational waves (LVK), ultra-faint dwarf galaxies (UFDGs), supermassive black holes (SMBHs), core/cusp (C-C) profiles for inner galactic halos. Figure taken from [23].

with m_1, m_2 being the binary component masses.
The time to the coalescence of a binary emitting GWs at a frequency f is given by:

$$\tau_c = 93.9 \left(\frac{f}{30\text{Hz}}\right)^{-8/3} \left(\frac{M_{ch}}{0.87 M_\odot}\right)^{-5/3} \tag{3}$$

where M_c is the *chirp* mass defined as:

$$M_c = (m_1 m_2)^{3/5} (m_1 + m_2)^{-1/5} \tag{4}$$

Immediately after the merger, the newly formed black hole oscillates in shape between a distorted, elongated spheroid and a flattened spheroid. This is called the ringdown phase, the distortion is damped by the emission of GW until the complete black hole relaxation.

The Advanced LIGO-Virgo Michelson interferometers are designed to detect such gravitational-wave signals. The interferometers consist of two perpendicular 4km long arms in which a laser beam circulates and is reflected at each end on mirrors. When a gravitational wave reaches one of the detectors, the associated stretching and compression of space generates a small difference in its relative arm lengths ($\sim 10^{-21}$ meters). The laser beam then has a different travel time in each arm, which means that the two beams are no longer in phase. This difference creates interference patterns that are measured at the output of the instrument. This is the gravitational-wave readout that can be seen in Fig.3. The maximum amplitude of the GWs is so small, that their detection above instrumental and environmental noise requires sophisticated processing pipelines to detect and extract the signals from the data [14], [15], [16].

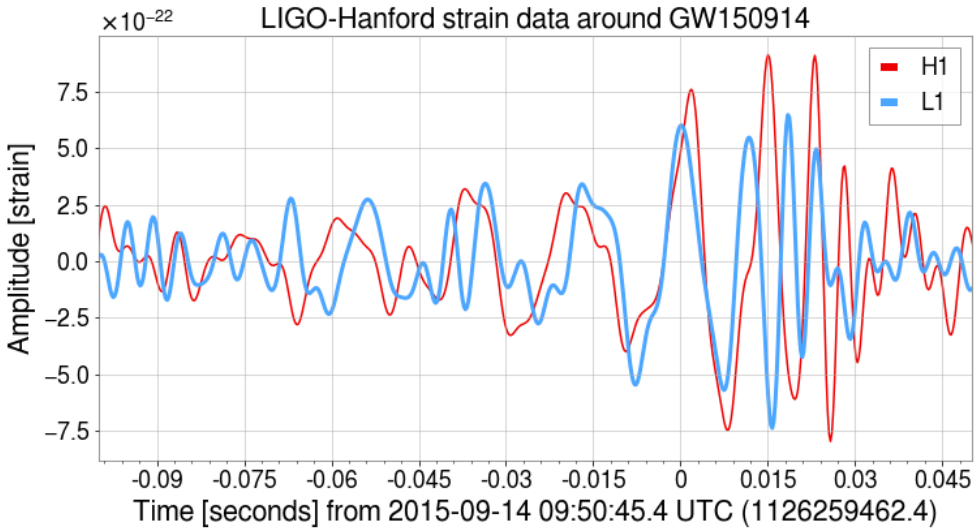

Figure 3: Superposition of the measured GW amplitude from the coalescence of two black holes in two LIGO detectors. The same signal is detected with a delay of ~ 7 ms related to the time needed for the GW to propagate from one detector (L1 -Livingston) to the other (H1- Hanford) separated by 3000 km.

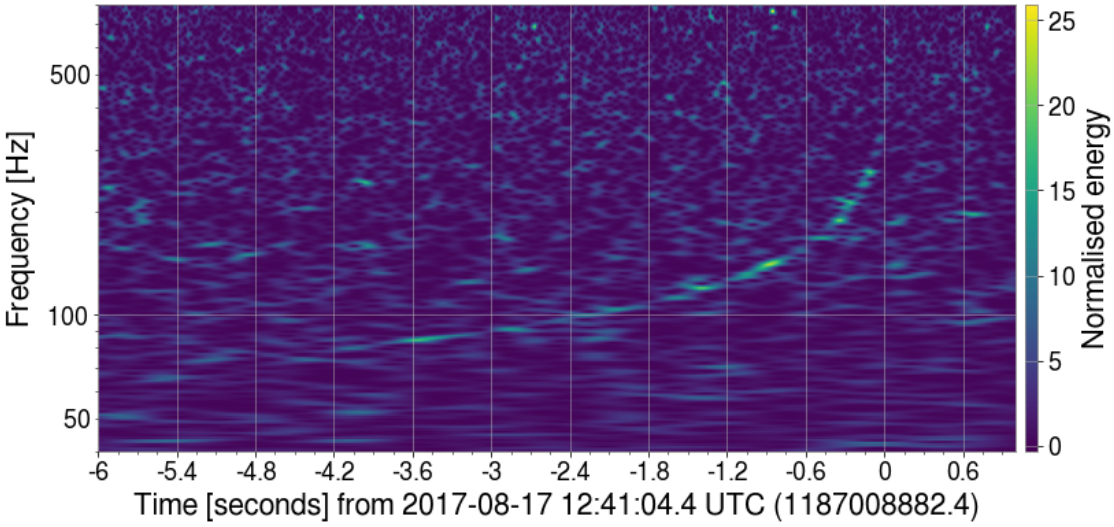

Figure 4: Spectrogram of the first detected signal from a binary neutron star coalescence(GW17017 in 2017). We observe the characteristic sweeping *chirp*.

Extract a gravitational wave signal from noise The data strain collected by the Advanced LIGO-Virgo detectors at the time of a GW event can be expressed as:

$$d(t) = h(t) + n(t) \tag{5}$$

where $d(t)$ is the detector's readout (the raw signal from the Michelson output) at time t, $h(t)$ is the GW signal we want to detect, and $n(t)$ regroups the many sources of noises for each detector (instrumental noise, thermal, seismic, quantum noise, among many others).

Matched filtering [25] is known to be the best technique to extract a signal of known form buried in stationary Gaussian noise. The technique basically compares the signal with various templates of *chirp* waveform h_T and finds a time when both match. Match filtering maximizes the signal-to-noise

(SNR) ratio at all times [24]:

$$SNR(t) = \frac{\langle h_T, d \rangle}{\rho_{opt}} \tag{6}$$

where t is the time at which the matching between filter and data is made and where the inner product $\langle a, b \rangle$ is defined as :

$$\langle a, b \rangle = 4Re \int_{f_{min}}^{f_{max}} \frac{\tilde{a}^*(f)\tilde{b}(f)}{S_n(f)} e^{2\pi i f t}\, df \tag{7}$$

where $\tilde{a}(f)$ and $\tilde{b}(f)$ are Fourier transforms, and where $\rho_{opt} = \langle h, h \rangle$ corresponds to the optimal signal-to-noise ratio. $S_n(f)$ is the power density of the noise (PSD).
This technique requires a large number of templates (tens of thousands) to be checked against the real data. The SNR is evaluated at the output of the interferometer for all times and all templates h_T. We obtain SNR graphs for each time and for each template where a peak represents the time t at which the signal and the best template are well matched (see Fig.5). An event trigger is recorded when this SNR time series crosses a certain threshold (above ~ 8 [14]). After verifying the validity of this trigger as a true GW signal, it is promoted to the rank of GW event. An alert is sent out by the LIGO-Virgo-KAGRA Collaboration to the partner observatories, for the search of a potential electromagnetic counterpart at different wavelengths, in order to fully characterize the emitting source.

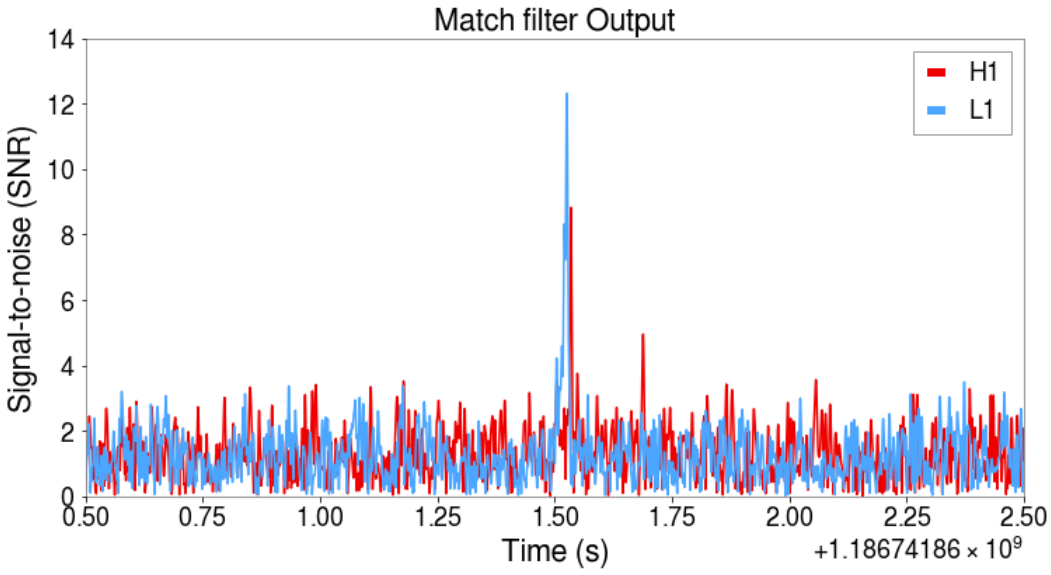

Figure 5: Zoom on the match filtering output around the merger time for GW140915 in the two detectors. The high peak corresponds to the time of the best match between the template waveform h_T used as the filter and the real waveform embedded in the detector noise.

The PSD, $S_n(f)$, characterizes the detector's output in the absence of gravitational wave signals. This PSD is used for match filtering as well as for the post-analysis of the data. It is a crucial quantity to evaluate in order to properly detect gravitational wave signals and infer the properties of the astrophysical sources that generated them. Inaccurate modeling of the noise can lead to incorrectly estimating the significance of an event and produce systematic biases in the estimation of the physical characteristics of the binary system.

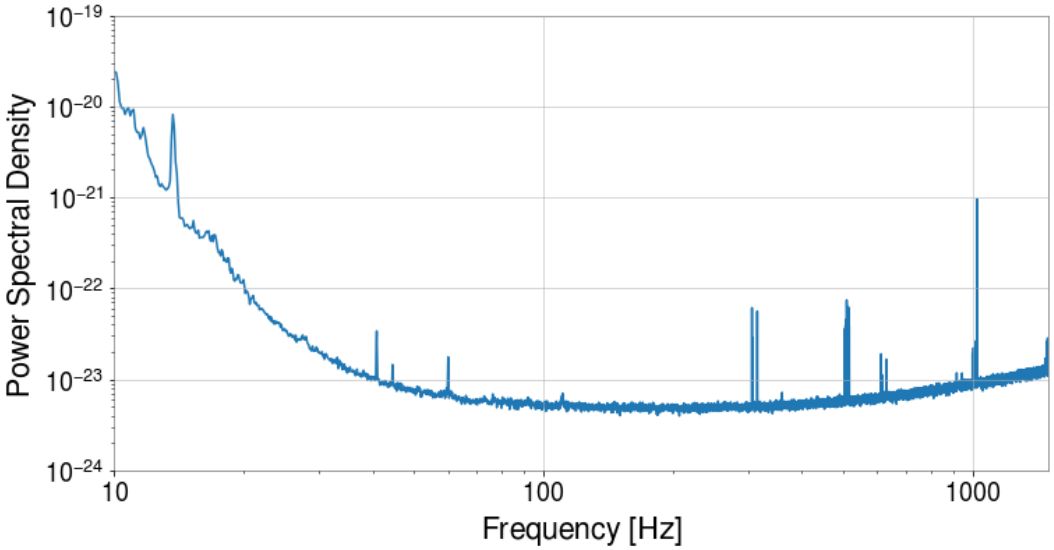

Figure 6: Power spectral density (PSD) $S_n(f)$ of the LIGO-Livingston detector. Low frequencies ≤ 30 Hz are dominated by noise related to the ground motion. The spikes or spectral lines confined to certain frequencies are typically caused by electrical/mechanical resonances. The best detector sensitivity is reached at around 100 Hz.

2 Method: Parameter Estimation of subsolar-mass binary black hole candidates

The goal of this work is to infer the physical parameters of the system that created the subsolar-mass binary black hole (SSM BBHs) candidate events of Table 1.
In the scope of this project, I focused on the SSMC1 candidate which is one of the most significant candidates in the search (the analysis of the second most significant candidate, SSMC2, is presented in Appendix B). As the aim is to determine if the candidate merger could come from subsolar-mass black holes, the most crucial parameter to estimate is the two masses of the binary components. We are also interested in finding pieces of evidence that the signals are really coming from a compact binary coalescence rather than from a non-astrophysical origin.

The SSM BBHs search performed by the LIGO-Virgo-KAGRA collaboration in [13] attribute a mass estimate for the candidate events' black holes (Table 1). These values correspond to the waveform template h_T that best matches the detected signal and have to be considered with caution. **A refined parameter estimation of the candidate's GW events must be made in the Bayesian framework to estimate the physical waveform parameters and quantify their uncertainties in order to accurately characterize the emitting system.** This is the standard procedure for any GW signal candidate but, here, adapted for very small mass black holes.

In the following Section is presented the method used to analyze and infer the physical characteristics of the candidates. In Subsection 2.1, I start by visualizing and cleaning the raw data in order to have the best data quality to apply the parameter estimation on the signal. Then, in Subsection 2.2, is presented the parameter estimation Bayesian framework chosen for the candidate along with the implementation of the analysis in Subsection 2.3. Lastly, in Subsection 2.4, I emphasize the choices made to reduce the computational cost of the parameter estimation without degrading the accuracy of the results.

2.1 Inspection and cleaning of the data

The data for the candidate signals are directly obtained from the O3b open-access data. In Fig.7 is shown the spectrogram of SSMC1 over 80 sec of data. The fact that the usual *chirp* signal can not be spotted by eye (compared to the binary neutron star event in Fig.4) is expected for an event with small SNR and small masses as it deposits a small amount of power for a very long time.

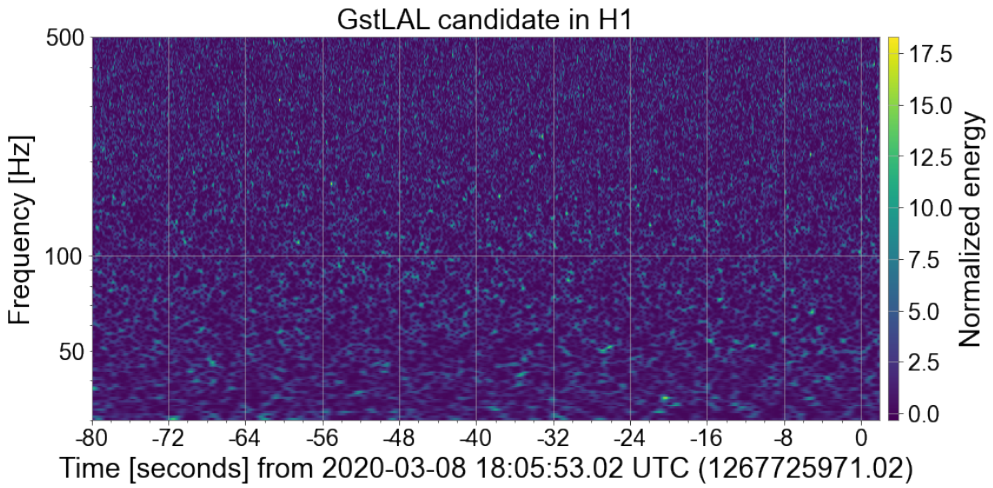

Figure 7: Spectrogram showing a 80 sec data segment before coalescence time t_c of the SSMC1 candidate data.

Gravitational-wave data contains numerous noise artifacts, called *glitches*, caused by a variety of sources such as instrumental issues in the detectors, earthquakes, or nearby human activity. Glitches are non-Gaussian transient sources of noise that take various shapes in the signals (example in Fig.8) and can be mistaken with real GW events or simply alter the parameter estimation of an event if located near. To visualize any of these short-duration noise features in our data I produce refined high-resolution time-frequency maps of the data segment to identify any of these transient noises [26].
After identifying the glitches in the data, one can create a model (reconstructed glitch waveform) using the `BayesWave` software [27] to fit and regress these undesirable non-gaussianities. This process of glitch subtraction, described in [28], basically consists in fitting the glitch in the data and subtracting it. One can see the efficiency of the removal in Figure 8 and 9.

2.2 Bayesian framework for parameter estimation of gravitational waves

The aim of Bayesian inference for gravitational wave astronomy is to construct a **posterior distribution** $p(\vec{\theta}|\mathbf{d})$, where $\vec{\theta}$ is the set of 15 parameters describing a binary black hole coalescence and $\mathbf{d}$ is the output data from a network of GW detectors. The posterior distribution is used to construct a credible interval around the value of these parameters that tell us, for example, the component masses of a binary black hole event. Inference of the physical parameters of the system $\vec{\theta}$ (such as masses or spins of the merging objects), relies on the knowledge of the generic shape of the GW signal as well as the distribution of the noise. Parameter estimation within the Bayesian framework allows one to perform a quantitative analysis of GW signals and to calculate

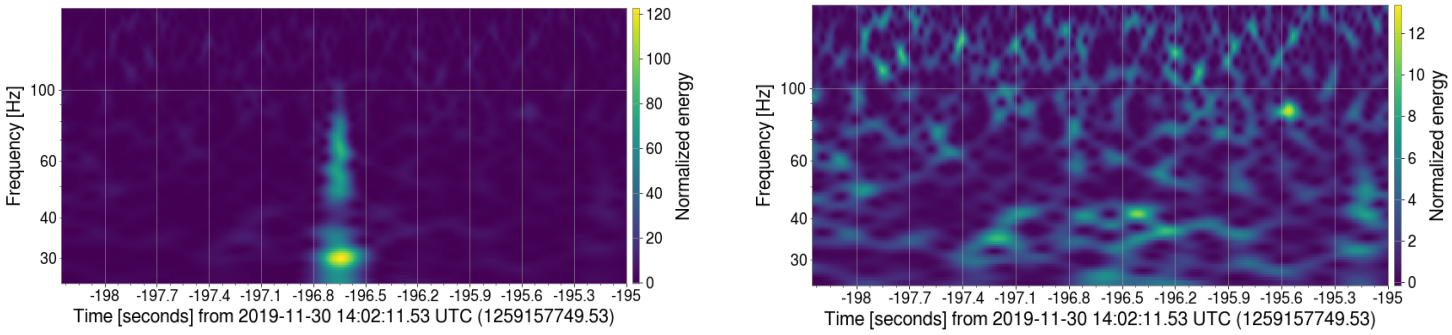

Figure 8: Left: Before glitch subtraction. The glitch deposits a high amount of energy compared to the background noise, in a short timescale (0.2 sec). **Right:** After glitch subtraction. One can notice that the normalized energy of the background noise is reduced by one order of magnitude.

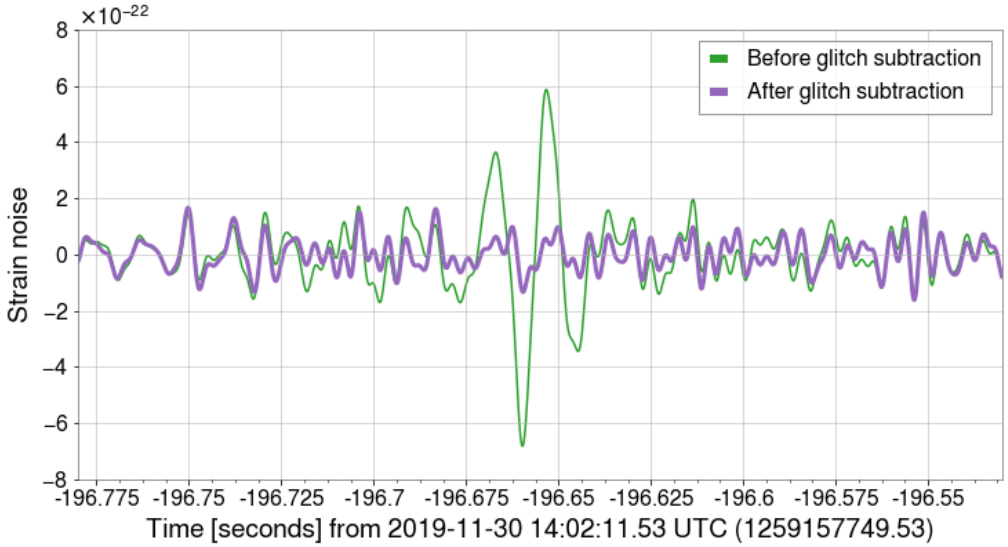

Figure 9: Subtraction of a glitch located -196 sec before the event. In green the original strain with a glitch at $\sim$ -196.65 sec and in violet the clean data after subtracting it with `BayesWaves`. Times are shown relative to the GW event GPS time.

the statistical significance of the physical parameters that best match the detected signal.

Given a model of the gravitational waveform shape $\mathbf{h}_T(\vec{\theta})$ that depends on the set of parameters $\vec{\theta} = \theta_1, \theta_2, ..., \theta_N$, and given a set of observations ($\mathbf{d}$ for data) and a hypothesis H (example: H_{GW}; there is a GW signal in our data, or H_{noise}; there is only noise), the posterior probability density function for $\vec{\theta}$ can be recovered with the Bayes Theorem:

$$p(\vec{\theta}|\mathbf{d}, H) = \frac{\Pi(\vec{\theta}|H) \cdot L(\mathbf{d}|\vec{\theta}, H)}{Z(\mathbf{d}|H)} \tag{8}$$

with the prior probability density function $\Pi(\vec{\theta}|H)$ the likelihood function $L(\mathbf{d}|\vec{\theta}, H)$ and the evidence $Z(\mathbf{d}|H)$ (the normalization constant of the posterior).

$$Z(\mathbf{d}|H) = \int d\vec{\theta}\, \Pi(\vec{\theta}|H) L(\mathbf{d}|\vec{\theta}, H) \tag{9}$$

Results for a specific parameter θ_i are found by marginalizing over the unwanted parameters. Indeed, the posterior distribution for a binary black hole merger is a fifteen-dimensional function that includes information about black hole masses, sky location, spins, etc, if we look at the posterior distribution for just one parameter θ_1, we marginalize (or integrate) over the parameters that we are not interested in:

$$p(\theta_1|d,H) = \int L(\vec{\theta}|d,H)\, d\theta_2 ... d\theta_N \tag{10}$$

This marginalized posterior distribution can be used to find the expectation of the parameter given its distribution, e.g., the mean:

$$\langle \theta_1 \rangle = \int \theta_1 \;\; L(\theta_1|d,H)\, d\theta_i \tag{11}$$

For gravitational wave applications, the data $\mathbf{d} = \mathbf{h} + \mathbf{n}$ consists of several time series of gravitational wave strain measurements containing the compact binary coalescence signal $\mathbf{h}$ and noise component $\mathbf{n}$. The gravitational signal $\mathbf{h}$ is a function of 15 parameters θ_k related to intrinsic and extrinsic characteristics of the merger event:

Intrinsic Parameters, fundamental properties of the binary

- Masses of the two black holes m_1, m_2.
- The spin vectors $\vec{s_1}, \vec{s_2}$ with spins magnitude a_1, a_2 and tilt angles θ_1, θ_2 between the compact objects' spins and the orbital angular momentum.
- Azimuthal angle separating the spin vectors θ_{12}.

Extrinsic Parameters, relative to the observer location and orientation

- Localization in the sky in celestial coordinates (right ascension α and declination δ).
- Luminosity distance of the source given by $d_L = \sqrt{\frac{L}{4\pi S}}$, where L is the bolometric luminosity and S, the bolometric flux.
- The angle θ_{JN} between the total angular momentum of the system and the line of sight.
- Time t_c at coalescence (when the amplitude of the signal is maximum).
- The orbital phase ϕ_c at the time of coalescence.

We can therefore write the parameter vector as $\vec{\theta} = \{m_1, m_2, \vec{s_1}, \vec{s_2}, \theta_{12}, \alpha, \delta, D_l, \theta_{JN}, t_c, \phi_c\}$.

The waveform template $\mathbf{h}_T$ for a specific GW signal can be modeled using post-Newtonian approximations. These models use post-Newtonian theory applied to the motion of a circular binary system. Indeed, the Newtonian approximation fails to describe accurately the orbits of a compact binary coalescence. The post-Newtonian theory allows one to add relativistic corrections to the equations of motion of a binary black hole system (we assume small velocities and weak gravitational field). It provides a powerful tool to model the inspiral stage of the system.

The choice of priors distribution for the parameters is an important factor in Bayesian inference and will affect the evidence and posterior estimation. Priors on those parameters are assigned based on astrophysical or detector properties. Usually, the priors on masses and spins of the

binary's components are set uniform. When we do not have prior beliefs about the parameters, we often choose a distribution that is uniform. The sources of coalescence signals are expected to be uniformly distributed, which is translated by a mathematical constraint on the declination $\Pi(\alpha, \delta) \propto \cos(\delta)$ where δ takes values between -$\frac{\pi}{2}$ and $\frac{\pi}{2}$.

The Likelihood function corresponds to the conditional probability to obtain the data strain $\mathbf{d}$ given a waveform model and a set of model parameters $\vec{\theta}$. The likelihood function is a chosen description of the measurement $\mathbf{d}$ so, by writing down a likelihood, we implicitly introduce a noise model. The noise in the detectors is assumed to be stationary and Gaussian, therefore in the absence of a signal the data should follow a zero mean Gaussian distribution. Therefore the likelihood of the data, under this assumption H_{noise}, and considering the noise uncorrelated between the different detectors, is :

$$p(\mathbf{d}|\vec{\theta}, H_{noise}) = \prod_{k=1}^{detectors} e^{-\frac{1}{T}\,(\tilde{\mathbf{d}}^{(k)*}\, S_n^{(k)-1} \tilde{\mathbf{d}}^{(k)})} \tag{12}$$

where T is the data segment duration $S_n(f)$ corresponds to the PSD (recall that in the absence of a signal, the simplest model which we consider is that of Gaussian, stationary noise with a certain PSD $S_n(f)$ and zero mean), $\tilde{\mathbf{d}}$ the Fourier transform of the data.

In the presence of a GW signal, the data can be described as $\mathbf{d} = \mathbf{n} + \mathbf{h}$ (hypothesis $H_{GW+noise}$), then the likelihood takes the form of the residual between the data and the matching template $\mathbf{d}$ - $\mathbf{h}(\theta)$. In the presence of a signal, this residual should be Gaussian distributed, therefore likelihood function is simply:

$$p(\mathbf{d}|\vec{\theta}, H_{GW+noise}) = \prod_{k=1}^{detectors} e^{-\frac{1}{T}\,(\tilde{\mathbf{d}}^{(k)}-\tilde{\mathbf{h}}^{(k))*}\, S_n^{(k)-1} (\tilde{\mathbf{d}}^{(k)}-\tilde{\mathbf{h}}^{(k)})} \tag{13}$$

where $\tilde{\mathbf{h}}$ is the Fourier transform the waveform template.

Nested Sampling Once the parameters, their priors, and the likelihood are specified, the next step of Bayesian inference is to compute the posterior distribution of $\vec{\theta}$. The posterior distribution is a complex structure of 15 dimensions with non-Gaussian features and complicated correlations. To compute robustly the posterior distribution of GW event parameters, stochastic samplers are usually used as the Nested Sampling algorithm, a method introduced by John Skilling in 2004 [29]. Different from the Monte Carlo Markov Chain methods that are designed to draw samples from the posterior distribution, Nested Sampling is designed to compute the evidence $Z(\mathbf{d}|H)$. The evidence is the normalization factor of eq.8 and corresponds to the integral over the entire parameter space, it is a highly dimensional integral. The key idea of Nested Sampling is that this high-dimension problem can be ingeniously mapped into an easier 1D integration problem. As a by-product, the posterior distribution of the parameters of interest can be reconstructed by weighting each of the samples used to calculate the evidence by the posterior probability of the sample. Details on the nested sampling theory and algorithm to compute the evidence and the posterior are presented in Appendix C with illustrating figures.

2.3 Parameter Estimation set-up

I perform parameter estimation for two subsolar-mass black hole candidates, SSMC1 and SSMC2, but in the following sections, I focus on the SSMC1 candidate (SSMC2 analysis is presented in Appendix B). I use the `LALInference` software [30], containing a C library with several post-processing tools written in Python, and providing a standard method for accessing GW detector data, characterizing detector noise, and generating waveform model templates. I also use the Nested Sampling routine of the software `BILBY` [31].

In order to infer the parameters of the SSMC1 candidate I need to specify:

- The parameters $\vec{\theta}$ to estimate along with their prior distribution $\Pi(\vec{\theta})$.
- A waveform template that can model our GW signal.
- The likelihood -the conditional probability to obtain the observed data around our candidate trigger time given this waveform model and the set of model parameters $\vec{\theta}$.

Parameters $\vec{\theta}$ A compact binary coalescence is described by the parameter vector: $\vec{\theta} = \{m_1, m_2, \vec{s_1}, \vec{s_2}, \theta_{12}, \alpha, \delta, d_l, \theta_{JN}, t_c, \phi_c\}$. Other choices of parametrization can be made to influence the efficiency of the posterior evaluation. The most efficient parametrizations minimize the correlations between the parameters and the number of isolated modes of the posterior. Instead of estimating the binary component masses m_1, m_2, the posterior for the chirp mass M_c (defined in eq.4, corresponding to a reparametrization of the mass plane) and the asymmetric ratio $q = \frac{m_2}{m_1}$ are evaluated. The individual masses can be recomputed from these two quantities. More details on this choice are in Appendix E. All of the other intrinsic and extrinsic parameters previously detailed in section 2.2 are kept. The list is given in Table 2.

Prior distributions The role of the priors is to specify the ranges of the model parameters and the beliefs about their probability distribution before the data are analyzed. If the priors are very wide, we are sure not to bias our parameter estimation but on the other hand, the parameter space to explore is greater leading to a much slower convergence. The priors, presented in Table 2, are purposely chosen uninformative and wide on the 15 parameters to bias as less as possible the parameter estimation. For most of the parameters, we use uniform priors on all their possible values. For the sky location of the binary, the weight of each patch of sky is set equally probable. The prior on M_c was intentionally set in a narrow range around the expected chirp mass from the search. Given that the relative error that can be expected in chirp mass is around $1/N_{cycles} \sim 1/18000 \sim 10^{-5}$ (see in Appendix E for the details), it is hard for the sampler to find the extremely narrow peak in chirp mass. If, at the end of the parameter estimation, the posterior distribution of the chirp mass is narrower than this prior zoom then one can conclude that the prior should not bias the shape of the posterior.

Waveform h In analyzing the data, I choose the waveform template `IMRPhenomPv2` [30] to fit our candidate GW signal. The waveform is a widely used model that describes very accurately the inspiral phase of a compact binary coalescence. It is one of the best templates of phenomenological waveforms to describe binary black hole mergers with spins and spin precession.

Likelihood The likelihood corresponds to the standard likelihood function for GW data of eq.13. The classic method to evaluate S_n, the power spectral density (PSD) of a signal, is to perform a (fast) Fourier Transform (FFT) on the data. However, as the GW data contains highly variable

Parameters	Range	Distribution
Chirp mass M_c	(0.2 $M_\odot$, 2 $M_\odot$)	Uniform
Mass ratio	(0.05, 1)	Uniform
Component spin magnitude a_1, a_2	(0,1)	Uniform
Spin tilt angles θ_1, θ_2	(0,π)	Sine
Difference between azimuthal spin angles: θ_{12}	(0,2π)	Uniform
Phase between orbital and total angular momentum ϕ_{jl}	(0,2π)	Uniform
Inclination of the orbit θ_{JN}	(0,π)	Sine
Orbital phase ϕ_c	(0,2π)	Uniform
Geocentric time t_c	trigger time + (0.2s, -0.2s)	Uniform
Luminosity distance d_l	(5Mpc, 300Mpc)	Uniform Volume
Right ascension α	(0,2π)	Uniform
Declination δ	(-π/2,π/2)	Cosine

Table 2: Priors of the parameters for the Bayesian parameter estimation.

noise (instrument glitches and environmental noise), it is preferable to average several shorter FFTs together to build the S_n. To compute the power spectral density I use Welch's method [32]. Welch method computes the PSD by, first, dividing the data into overlapping segments, multiplying each segment's signal by a window function and performing an FFT on each, and finally averaging the amplitude reported in each frequency bin across each FFT.

2.4 Trade off between running time and accurate parameter estimation

How much time of strain data should be analyzed? Ideally, we would like to perform the parameter estimation on the whole GW signal, meaning that we would need to start the analysis when the waveform signal has a low frequency of around 20 Hz. With the analytical formula eq.3 one can estimate the duration needed to analyze the signal if starting the analysis when the waveform frequency is at $f = f_{low}$ before the coalescence time t_c where $f = f_{isco}$. We see that to avoid the data segment duration being very large ($<$ 200sec), leading to a subsequently higher convergence time, it is possible to start the parameter estimation at $f_{low} >$ 20Hz. This low-frequency cut-off leads to a loss in the quality of the signal which is evaluated in Fig.10.
I choose to set $f_{low} = 50$ Hz which reduces considerably the data segment duration to ~ 130 sec with a reasonable loss of $SNR_{loss} < 10$ % (see Fig.10).

Convergence Time When initializing the Nested Sampling routine one need to choose a number of live points to sample the parameter space. Increasing the number of live points increases the accuracy of the evaluation of the posterior, however, it also tremendously increases the convergence time of the sampler. The number of posterior samples generated by the Nested sampler is proportional to the number of likelihood evaluations during the process, which is directly related to the number of live points N. To have an idea of the duration to convergence, one can evaluate the time taken to evaluate one likelihood for one live point (for our data it is about 0.1s). As the typical number of likelihood evaluations for the parameter estimation of a long GW signal can take up to 10^6 likelihood calls to reach convergence, we should not choose N $>$ 500 to reach the convergence in a reasonable amount of time (less than a month).
Another option is to take advantage of our access to the multiple processors on the LIGO cluster and run parallel Nested Sampling. When running the sampler in parallel with identical configuration and data, each sample from the prior distribution can be treated as being part of a collection of $N_T = \sum_{k=1}^{N_{runs}} N_k$ samples – where each parallel run has N_k live points. As so, parallelism allows to

artificially increase the number of live points without adding too much additional run-time.
I set $N_k = 500\ \forall k$ and $N_{run} = 16$, the nested sampler reached convergence after 1 month and a half.

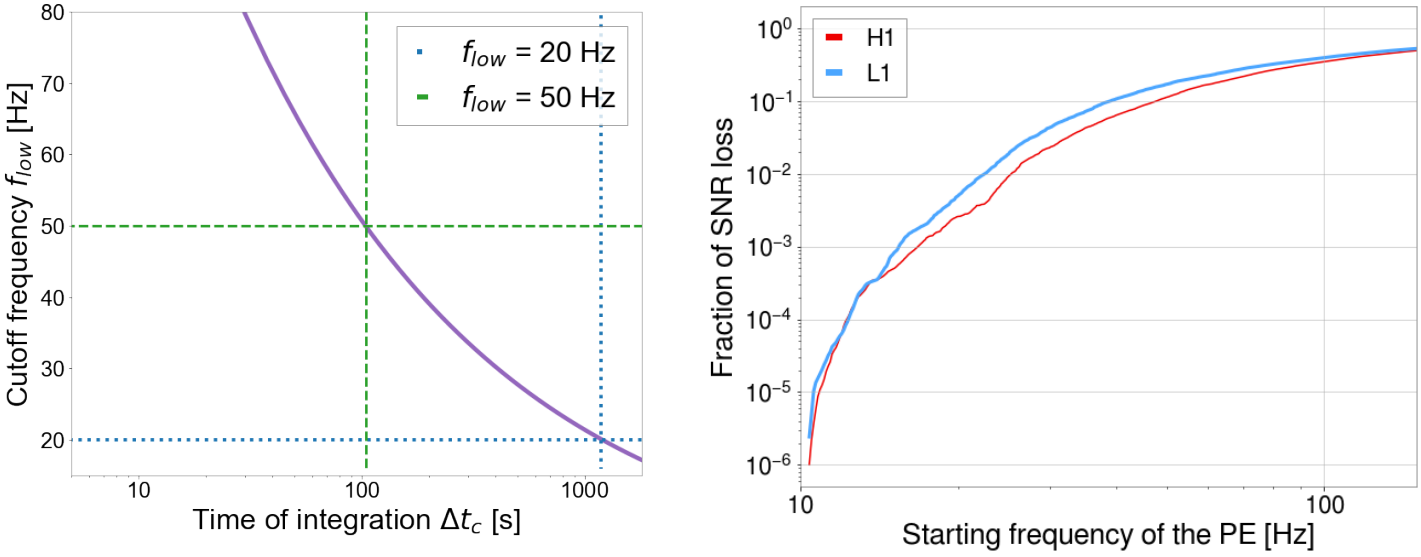

Figure 10: Left: Duration Δt_c of the signal in the detector depending on the starting frequency of analysis f_{low}. For example, if we start to analyze the signal from $f_{low} = 50$ Hz the total duration of the signal is $\Delta t_c \sim 130$-sec, with $f_{low} = 20$ Hz it is $\Delta t_c \sim 1000$-sec long. **Right:** Fraction of SNR lost when starting the parameter estimation (PE) at different frequencies. SNR loss <10 % of optimal SNR with $f_{low} = 50$ Hz. Details on the making of this graph in Annex D.

3 Results and Discussion

3.1 Physical properties of the candidate SSMC1

Parameter estimation with Nested Sampling allows us to recover the global posterior distribution of SSMC1 physical parameters. From this 15N-dimensional posterior, we can generate the marginalized probability for each of the parameters θ_i. For any subset of parameters, one can also visualize the output of the parameter estimation by constructing *corner plots*, to show the marginalized two-dimensional posterior probability distributions of correlated parameters. Table 5 summarizes the values found for several significant parameters of SSMC1. As the source is located at cosmological distances, all the measures are redshifted (e.g $m_{obs} = (1+z)m_{source}$). In the following section and in Table 5 is presented the source values for the signal's parameters, corrected from this redshift.

Masses In Figure 11 is shown the posterior distribution of the SSMC1's component masses (the priors on these masses were uniform between 0.1 and 2 solar mass). SSMC1's source corresponds to a subsolar-mass event with individual source-frame masse $m_1 = 0.53^{+0.32}_{-0.11}$ $M_\odot$ and $m_2 = 0.29^{+0.07}_{-0.10}$

$M_\odot$; for each parameter, we report the median value and the 1-sigma error bars. The median is chosen as a measure of central tendency because it is a robust estimator that is less affected by outliers or asymmetry in the distribution. These values are coherent with the one found by the search (in Table 1; $m_1 = 0.78$ $M_\odot$ and $m_2 = 0.23$ $M_\odot$). The marginalized posterior distribution for the first mass favors a mass lower than 1 $M_\odot$ at 97% and for the second mass at 100 %. The two compact objects are not of equal mass, their mass ratio $q = \frac{m_2}{m_1}$ is bound to the range $0.25 \leq q \leq 0.82$. These component masses were computed using the chirp mass M_c and the mass ratio q (Fig.11. The chirp mass posterior is tightly constrained with $M_c = 0.34^{+0.01}_{-0.01}$, indeed we expect it to be the best constrained among the source parameters as it is the dominant quantity in setting the frequency and phase evolution of the GW signal and is well measured for low mass binaries which have a long inspiral[1]. The mass ratio q is instead harder to measure, tending to increase the incertitude on the component masses. The parameter estimation results on the component masses of SSMC1 show their subsolar origin with great certainty.

Distance and orientation The luminosity distance d_L and inclination angle θ_{JN} posterior distributions are shown together in Figure 12, with d_L given in Mpc, and θ_{JN} in radians. θ_{JN} corresponds to the angle between the system's total angular momentum and the direction of propagation from the source to the observer. The two parameters are correlated [2]. The corner plot shows a clear bimodal distribution for θ_{JN} due to the fact that one can not distinguish whether the system is being observed face-on ($\theta_{JN} \sim 0$) or face-away ($\theta_{JN} \sim \pi$), nevertheless the system being edge-on ($\theta_{JN} \sim \pi/2$) seem disfavoured.

GW observations are directly sensitive to the luminosity distance to a source, but not the redshift. One can use the inferred luminosity distance along with the Hubble parameter and matter density parameter (from Planck15 [19]) to compute the posterior distribution for the redshift of the source[3]; $z = 0.03^{+0.02}_{-0.01}$.

Spins Spins are a fundamental property of black holes. Their magnitude and orientation with respect to the orbital angular momentum are very informative about the origin and formation history of the binary. To characterize the spin configuration of a binary back hole event, the effective spin parameter χ_{eff} is commonly used:

$$\chi_{eff} = \frac{\frac{\mathbf{S_1}}{m_1} \cdot \frac{\mathbf{S_2}}{m_2}}{m_1 + m_2} \cdot \hat{L} \tag{16}$$

where $\mathbf{S_1}$ and $\mathbf{S_2}$ are the BHs' spin normalized by the maximum spin of a rotating black hole ($\frac{GM^2}{c}$) and $\hat{L}$ is the direction of the angular momentum. χ_{eff} is a conserved quantity throughout the inspiral phase of the merger, it is a dimensionless number ranging from -1 to 1, where if χ_{eff} = 1 the spins of the compact objects are aligned with their orbit, and if χ_{eff} = -1 the spins are

[1]The GW signal phase evolution is driven the chirp mass : $\dot{f}_{gw} = \left(M_c(1+z)\right)^{5/3} \cdot f_{gw}^{11/3}$ [24]

[2]The luminosity distance between the binary emitting GW and the detector can be approximated as:

$$d_l \sim 4\pi^{2/3} \frac{G^{5/3} M_c^{5/3} f^{2/3}}{c^4 \cdot h \cdot (1 + \cos^2(i))} \tag{14}$$

where h is the amplitude of the GW signal and i is the angle between the line of sight and the normal direction with respect to the orbital plane.

[3]

$$d_l(z) = \frac{c(1+z)}{H} \int_0^z \frac{dz'}{\sqrt{\Omega_m (1+z')^3 + \Omega_\Lambda}} \tag{15}$$

with H the Hubble parameter, c is the speed of light, Ω_m the matter–energy fraction of the Universe, and Ω_Λ [33]

perfectly anti-aligned. $\chi_{eff} \sim 0$ can mean that the magnitude of the spin parameters is $\ll 1$ or indicates a formation channel where spins are largely uncorrelated with their orbit. This is the case for BBHs formed dynamically in dense stellar environments and for PBHs [34], which additionally are predicted to have small intrinsic spins. SSMC1 seems to have a $\chi_{eff} \sim 0$, which is coherent with a PBH origin scenario.

In Figure 12 is plotted χ_{eff} along with the effective precession spin parameter, χ_p, which is a measure of the component masses spins parallel to the orbital plane. A value of $\chi_p \sim 0$ would indicate no spin precession of the orbital plane and a value of $\chi_p = 1$ a maximal precession. However, the posterior of χ_p is not very informative with a broad confidence interval $0.19 \leq \chi_p \leq 0.7$.

Parameter	Values
Primary mass ($M_\odot$)	$0.53^{+0.32}_{-0.11}$
Secondary mass ($M_\odot$)	$0.29^{+0.07}_{-0.10}$
Final mass ($M_\odot$)	$0.82^{+0.16}_{-0.04}$
Mass ratio ($m_2/m_1 < 1$)	$0.55^{+0.3}_{-0.27}$
Chirp Mass	$0.34^{+0.01}_{-0.01}$
χ_{eff}	$-0.05^{+0.23}_{-0.30}$
χ_p	$0.42^{+0.28}_{-0.23}$
Luminosity Distance (Mpc)	$155.75^{+88.75}_{-65.76}$
Redshift	$0.03^{+0.02}_{-0.01}$
Global SNR	8.90
P($m_1 < 1\ M_\odot$)	97%
P($m_2 < 1\ M_\odot$)	100%

Table 3: Results of the parameter estimation for SSMC1. All masses are in the source frame. The statistical uncertainty of all the parameters is quantified by the 68% credible intervals about the median of the marginalized one-dimensional posteriors.

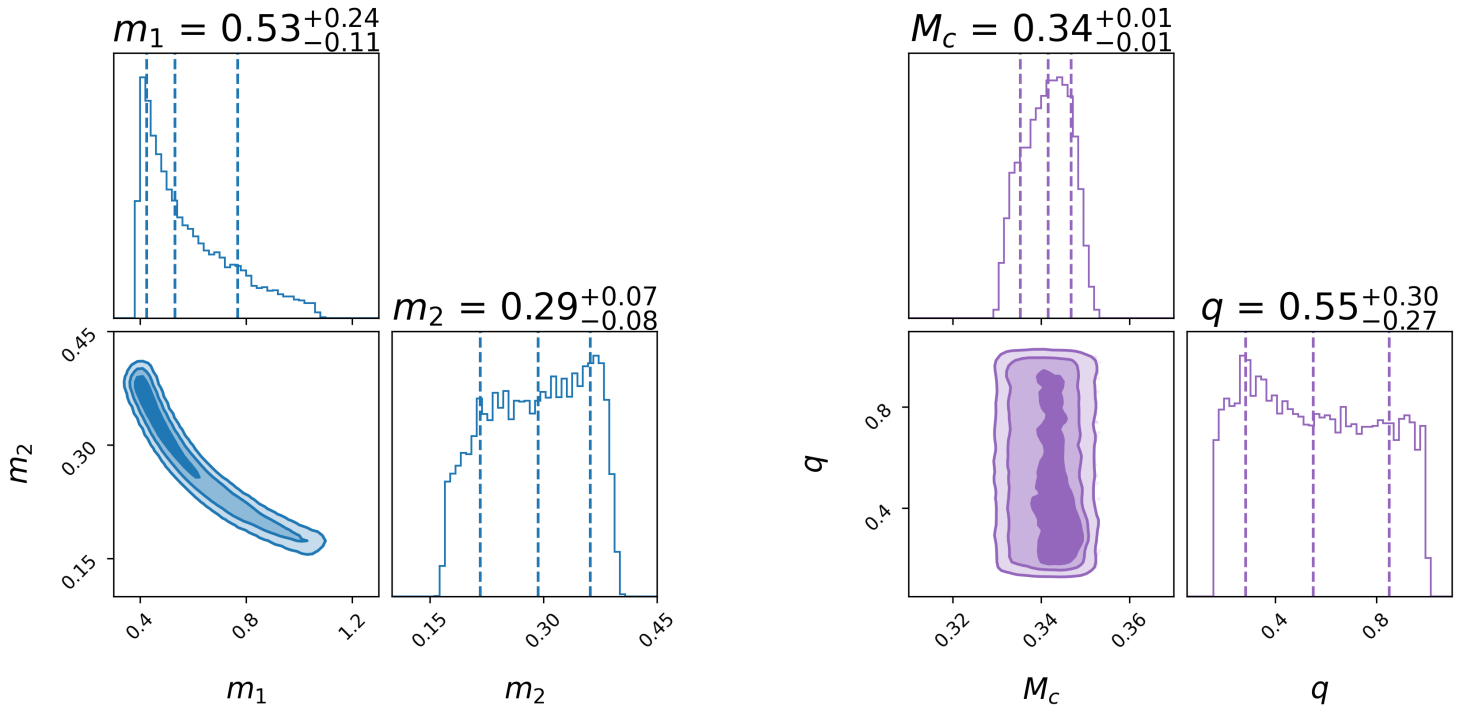

Figure 11: Left: Corner plot for the black hole masses. The marginalized distribution for each parameter is shown in the histograms. For each parameter is reported the median value and 1-sigma error. The contours of the joint posterior distribution correspond to the range of the symmetric 39%, 86%, and 99% credible interval with respect to the median. **Right:** Corner plot for the chirp mass and mass ratio.

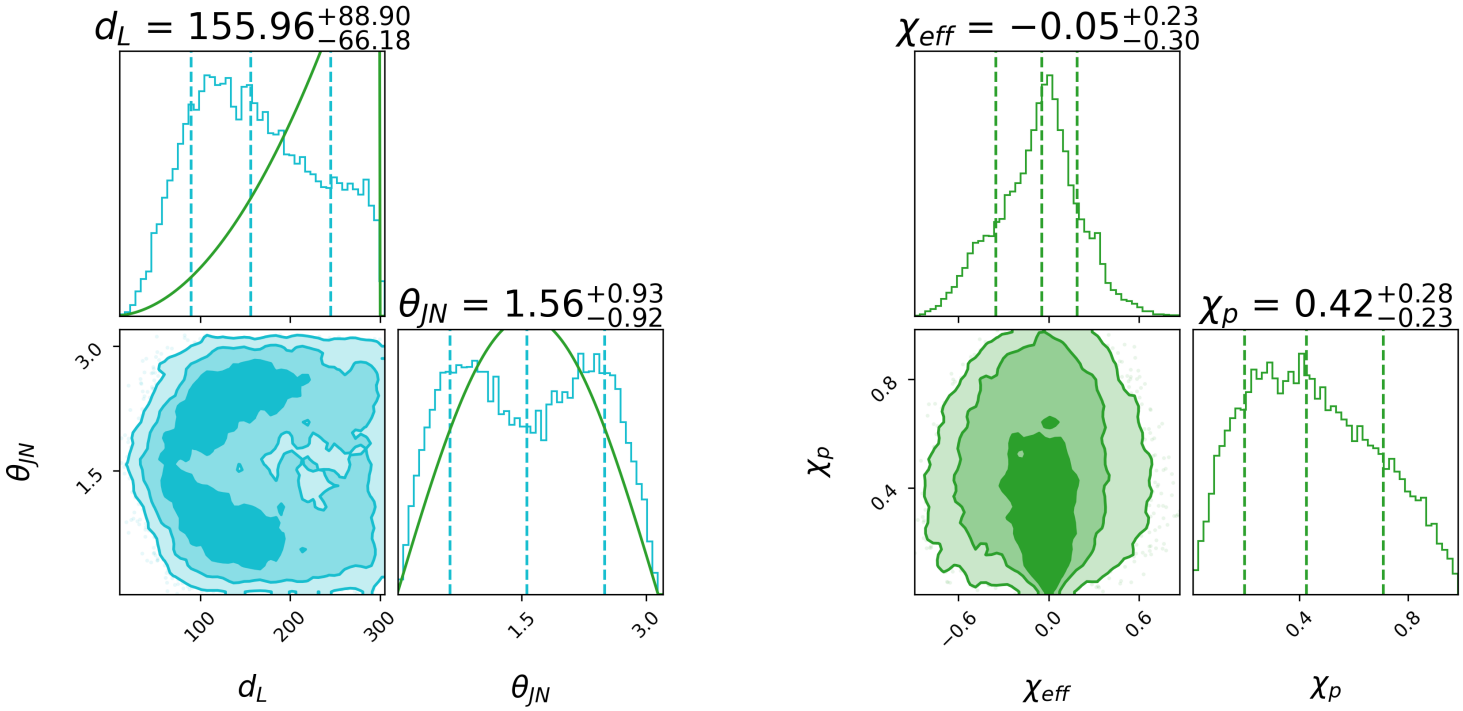

Figure 12: Left : Corner plot for the luminosity distance and θ_{JN}. In green are shown the prior distribution for d_L -uniform-in-volume prior between 5 and 300 Mpc- and θ_{JN}. **Right :** Corner plot for χ_{eff} and χ_p.

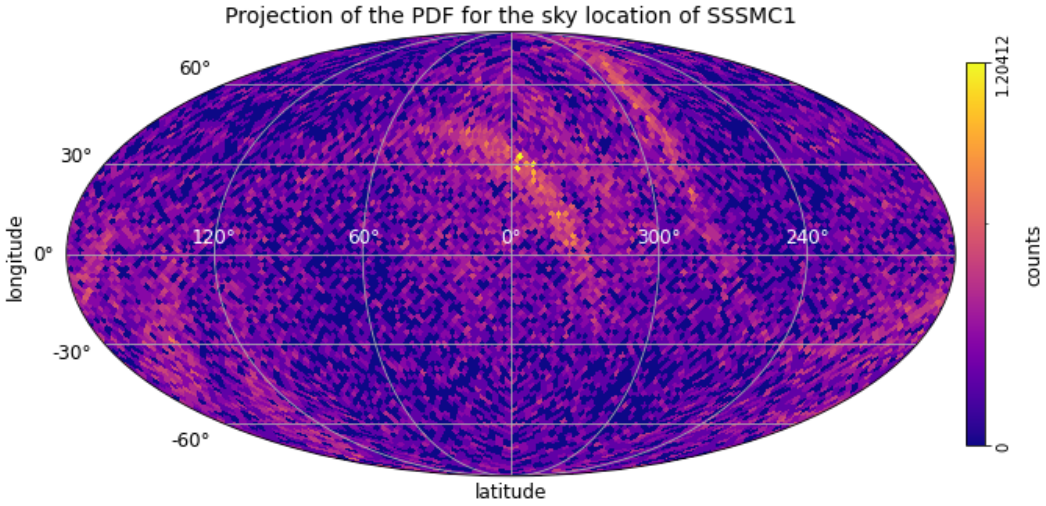

Figure 13: Posterior of the sky location of the signal source in Galactic Coordinate (with the Galactic center in the middle).

3.2 Significance of SSMC1

In this subsection, I explore different methods to assess the significance of SSMC1. The goal is to discriminate if SSMC1 is more likely to be of noise origin or a real astrophysical GW signal. As the results of parameter estimation show with great confidence the subsolar-mass origin of the binary components, if the second hypothesis is favored, this would have huge implications for astrophysics and fundamental physics.

Candidate significance The search for subsolar-mass black hole binaries performed by the LVK collaboration and presented in Table 1 [13] shows that SSMC1 is a promising candidate. With its low false-alarm rate (FAR) of 0.2 yr^{-1} and its global signal-to-noise ratio of 8.9, the candidates is comparable to several confirmed events of O3b with similar SNR and FAR; e.g. GW191127 with FAR of 0.25 yr^{-1} and SNR 10.3 or GW191230 with FAR 0.42 yr^{-1} and SNR 9.9 [2].
In addition, the false alarm probability (FAP) of this candidate is:

$$\texttt{FAP} = 1 - \exp(-\texttt{FAR} \cdot T_{obs}) \tag{17}$$

given that the time of operation with at least two detectors observing for O3b is $T_{obs} = 125.5$ days [2]. Therefore, purely according to the search, the candidate has a 6.5% probability of having a noise origin.

Insights from the parameter estimation results The results of our parameter estimation show posterior distributions for SSMC1's parameters that are consistent with a real GW signal. Indeed, running parameter estimation on a strain of data containing only noise and no GW signal leads to (i) a very chaotic convergence of the nested sampler and (ii) prior dominated posterior distributions or the parameter. (ii) means that the marginalized posterior distribution of the parameters would overlap the prior; for example, in Fig. 11 the posterior masses would be uniformly distributed between 0 and 2 $M_\odot$. The analysis of SSMC1 shows no evidence of prior dominated parameters, the best example being θ_{JN} which has a clear bimodal distribution compared to its Gaussian prior (Fig. 12).

Bayes Factor The evidence computed with the Nested Sampling algorithm is primarily used to retrieve the posterior distribution of the coalescence parameters. This quantity is also used to do model selection, answering the question: *which model is statistically preferred by the data and by how much?* [35]
We want to compare a *signal model*, in which we suppose that there is a compact-binary-coalescence signal present in the data, to the *noise model*, in which we suppose that there is only Gaussian noise and no GW signal. The Bayes Factor allows us to discriminate one model over the other using their evidence:

$$B_{S,N} = \frac{Z^S}{Z^N} \tag{18}$$

where Z corresponds to the evidence:

$$Z(\mathbf{d}|H) = \int d\vec{\theta}\,\Pi(\vec{\theta}|H)L(\mathbf{d}|\vec{\theta},H) \tag{19}$$

with $Z^S = p(\mathbf{d}|H_S)$ the likelihood of eq.13. While the *signal model* is described by the fifteen binary parameters $\vec{\theta}$, the *noise model* is described by no parameters. Thus, we can write the noise evidence as the *null likelihood* $Z^N = p(\mathbf{d}|0)$ with eq. 12.

How does the Bayes Factor can help us to discriminate one model over the other? The Bayesian evidence $Z = \int d\vec{\theta}\,\Pi(\vec{\theta}|H)L(\mathbf{d}|\vec{\theta},H)$ encodes two pieces of information: the likelihood describes how well our model fits the data, and, when marginalizing it, gives us information about the size of the volume of parameter space used to carry out this fit. As we want to get the best fit possible but with a minimum prior volume, a model with an acceptable fit and a small prior volume often yields greater evidence than a model with an excellent fit and a huge prior volume. As so, the Bayes factor penalizes the most inaccurate and/or complicated model [36].

One model is preferred over the other when the absolute value of $\log(B_{S,N})$ is large. Usually, a threshold of $\log(B_{S,N}) > 2-3$[37] is used to claim a GW signal detection, and a threshold of $|\log(B_{S,N})| = 8$ is often used as the level of strong evidence in favor of one hypothesis over another. A negative $\log(B_{S,N})$ would indicate that the *noise hypothesis* is favored.
For the **SSMC1 candidate, the Bayes factor given with our parameter estimation is** $\log(\mathbf{B_{S,N}}) = \mathbf{0.4}$. This result shows a slight preference for the *signal model* but can not discard the *noise hypothesis*. To compare, when running a parameter estimation on strain of data containing only noise (no GW signal) we obtain $\log(B_{S,N}) = -0.1$.

Bayes coherence factor The Bayes Factor is the standard method used to evaluate the significance of GW detection [38], but in the case of low SNR and small masses it has been shown in [37] that this ratio performs more poorly. Therefore we need to use additional statistical factors to assess the significance of our subsolar mass candidate.

In [37] and [39] has been developed a new *coherence test* which can discriminate between a *signal coherent model* and a *incoherent signal model*. A coherent signal is characterized by a simultaneous arrival in the detectors up to a fight time delay and a good description by a compact-binary-coalescence (CBC) waveform. In contrast, if instead of a CBC signal, we are in the presence of simultaneous glitches mimicking a GW event, the detected signal should not be expected to fully satisfy these criteria. The Bayesian coherence ratio (BCR) computes the odds between the hypothesis that a coherent CBC signal is present in the data H_S and the hypothesis that instead, the data presents incoherent instrumental features. Those instrumental features can

be of two natures; each detector has either a glitch in Gaussian noise (H_G) or pure Gaussian noise (H_N). For a network of D detectors:

$$BCR = \frac{Z^S}{\prod_{i=1}^{D} Z_i^N + Z_i^G} \tag{20}$$

Z^S is the same as above, Z_i^N corresponds to the noise evidence (eq.12) for a single detector, and Z_i^G models a glitch which appears exactly as a real GW would in a single detector.

The threshold at which we can consider that the coherent-signal hypothesis is favored depends on the BCR values obtained for a bunch of background glitches. The BCR computed for one data strain (with the same duration as SSMC1) containing sevral glitches and no GW signal is $\log(BCR) = -1$. Furthermore, according to [39], if we consider the intrinsic probabilistic meaning of the BCR, a value of $\log(BCR) < 0$ indicates a preference for the instrumental-artifact hypothesis over the coherent-signal one. **For the SSMC1 candidate, I obtain** $\log(BCR) = -0.047$**. This result, close to zero, does not allow us to draw a firm conclusion on the coherence or incoherence of the signal.**

As can be seen, the candidate SSMC1 cannot be categorized with certainty as coming from an astrophysical source or from instrumental noise. It is very likely that this uncertainty comes from the rather low signal-to-noise ratio of the candidate. Analyzing a longer portion of the signal ($>$ 200 sec) would most probably lead to a higher Bayes Factor and BCR. Indeed the Bayes factor scales as [40]:

$$\log(B_{S,N}) \propto SNR^2 \tag{21}$$

3.3 On the astrophysical origin of the signal

In this section, I explore the different astrophysical scenarios that could produce a subsolar-mass trigger in the detectors.

Neutron Stars The first possibility to consider in order to explain the subsolar-mass components of the candidate would be that they are two neutron stars. Here, the neutron star nature of SSMC1 compact objects seems disfavored. Indeed, it is known from observation of pulsars and X-ray binaries involving an accreting neutron star from a companion that the mass range of neutron stars spans between 1.25 and 1.45 $M_\odot$ [41] [42]. This was further confirmed by the observation of the first neutron star binary event GW170817 [43]. Furthermore, recent core-collapse supernova simulations indicate that it should be difficult to form neutron stars with masses below 1.2 $M_\odot$ [44] [45]. Although the neutron stars' interpretation of the SSMC1 component masses seems unlikely, given the current limited knowledge of the neutron star's equation of state, it is not yet possible to exclude a neutron star origin. Additionally, it is very difficult to discard the black hole origin of a $< 3\ M_\odot$ gravitational wave event. Binary neutron star mergers or neutron star-black hole mergers can produce an electromagnetic (EM) signal counterpart which can be detected by LVK's partner observatories (Zwicky Transient Facility, Vera C. Rubin Observatory among others) to confirm the nature of the event. In the absence of detection of an EM-counterpart, the gravitational-wave data alone can not rule out the possibility that the objects are low-mass black holes [46].

Could Ligo-Virgo black holes be primordial? Shortly after the first detection of gravitational waves from a merger of $30M_\odot$ black holes by LIGO [1], it has been suggested that the

progenitors of this event could be two Primordial Black Holes [47] [4] [3]. The following GW events detections showed that the detected black holes tend to be more massive than those observed in black hole X-ray binaries [48]. Another anomaly lies in the pair-instability mass gap, theory predicts the existence of a gap in the black hole mass distribution because of pair-instability supernovae; black holes are not expected to form in the mass range of 50 to 130 $M_\odot$ [49] [50]. But some signals, such as GW190521 with two inspiralling black holes of about 85 and 66 $M_\odot$, have component masses within this predicted pair-instability mass gap.
Among other atypical GW events, there is the merger of a $m_1 = 23M_\odot$ black hole with a $m_2 = 2.6M_\odot$ compact object (event GW190814) with highly asymmetric masses and the lower-mass component m_2 lying between the heaviest known neutron star and the lightest known black hole in a compact-object binary [51]. Or some candidates' events of inspiral of a binary neutron star system, like GW190425, that have total masses substantially larger than any known Galactic neutron star binary [52]. The unusual characteristics of these events could be well explained if we consider that they are not classic stellar black holes but PBHs.
Another motivation to consider PBHs is the existence of supermassive black holes (SMBHs) at the center of galaxies. These $> 10^5$ $M_\odot$ black holes cannot yet be explained within the purely astrophysical mechanism, and PBHs could constitute the seeds for these SMBHs.

Could SSMC1's source components be Primordial Black Holes? On the other hand, many studies show that the thermal history of the Universe can enhance the formation of PBHs at different epochs [53][54]. PBH formation should have been boosted during the Quantum Chromodynamic (QCD) phase transition (t$\sim 10^{-6}$ sec in the early universe) generating a distribution of PBH masses sharply peaked around one solar mass (Figure 14). We would then expect to find a larger amount of PBHs with a mass around $1M_\odot$, leading to a possible enhanced rate of binary merger events in this mass range. Unusual events like GW190425 or GW190814 could be explained if its two components are not neutron stars or black holes but PBHs from the QCD peak [55]. The inferred characteristics of SSMC1 (and SSMC2 second mass, see Appendix B), if truly coming from a GW event, would be consistent with subsolar-mass black holes.

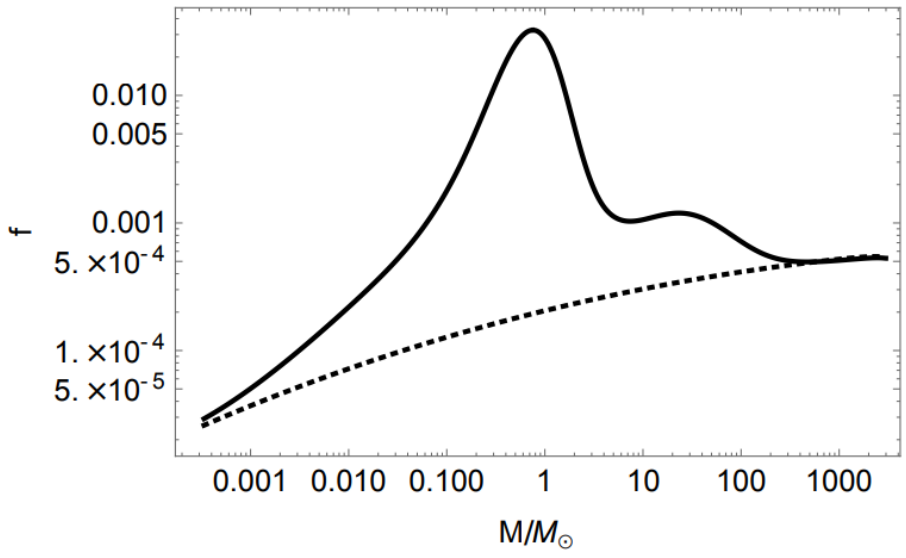

Figure 14: Predicted mass distribution f of PBHs formed during the QCD phase transition. A clear peak in the PBH distribution occurs at about 1 $M_\odot$. The straight dashed black line represents the mass function f of PBHs if there was no phase transition. Figure taken from [54].

4 Conclusion and Perspectives

In this work, I have performed an in-depth analysis of one of the most significant candidates reported in the O3b search for subsolar-mass black hole binaries [13] with SNR = 8.9 and FAR = 0.2 yr^{-1}. Even if the candidate does not show enough significance to claim the firm detection of a gravitational wave event, it is of great interest to study and characterize the signal. For this purpose, I first inspected and cleaned the data to remove any transient noise or glitch that could bias the analysis of the candidate. Then, I performed a parameter estimation with Nested Sampling to infer the value of the 15 intrinsic and extrinsic parameters describing the signal. The results are in agreement with the search performed by the collaboration. The inferred masses show that the signal, if coming from a GW event, is consistent with a binary of two subsolar-mass black holes; $m_1 = 0.53^{+0.32}_{-0.11}$ and $m_2 = 0.29^{+0.07}_{-0.10}$ $\mathrm{M}_\odot$ (1-sigma error bars) and $\sim 100\%$ confidence of being below one solar mass. In a second time, I investigated the significance of the candidate, trying to quantify the odds that the detected trigger comes from an astrophysical source rather than from a noise origin. Although the false alarm probability of the candidate is low (FAP = 6.5 %) and the results from the parameter estimation show good agreement with what one can expect from the analysis of a classic GW event, the Bayes Factor ($\log B_{S,N} = 0.4$) and Bayesian Coherence Factor ($\log \mathrm{BCR} \sim 0$) are too low to discard the noise hypothesis. Finally, I explored the different scenarios that could lead to the production of subsolar-mass signals such as SSMC1. Given the very low mass m_1 and m_2 of the candidate's components, their neutron star nature seems disfavoured by the recent observations and simulations, but this question remains open as the state equation of neutron star is not yet fully understood. On the other hand, the unusual characteristics of SSMC1 could be well explained by the two components being Primordial Black Holes. In addition, considering the PBH mass function, we expect to find a higher portion of the PBHs with masses around 1 $\mathrm{M}_\odot$.

It is highly probable that the significance of the candidate will improve when analyzing a longer portion of the signal (>130sec) which allows to capture the low frequencies of the signal. I am currently running a 220-sec parameter estimation that will converge after 2-3 months. Another path to explore to be able to discriminate the nature of the detected candidate would be to calculate an eventual tidal effect on the signal. If a binary contains at least one neutron star component, the GW signal is modified by the deformability of neutron star matter. This deformability can be quantified by the dimensionless quadrupole tidal deformability Λ_i, with black holes having $\Lambda_i = 0$. So far, the effect is so small that it has not been possible to place a lower limit on the tidal deformability on any of the O3b cataloged events [2]. One can expect that this parameter can be used in the future to distinguish between a binary black hole and a binary neutron star coalescence using only GW data.

As of today, the detectors' capabilities are at the limit of allowing the firm detection of a subsolar-mass black hole and claiming a PBH detection. We expect to detect future candidates with higher SNR that will not leave any ambiguity about the astrophysical nature of the signal and allow for precision measurement of the candidates' properties. The future data from LIGO-Virgo-KAGRA observing runs O4 and O5 (May 2023, 2027) and next-generation detectors such as LISA (launch in 2037) and the Einstein Telescope (first observations planned in 2035) will certainly offer a great opportunity to confidently identify subsolar binary black holes if they exist.

A Pipelines

In the linked document below I performed a literature review of the three main pipelines that are used to search for gravitational wave signals in the detectors' data (namely MBTA [15], GstLAL [14], and PyCBC [16]). Each candidate event is assigned a ranking statistic by the search pipeline that detected it. This ranking value is crucial to determine if a detector's trigger is more likely to originate from an astrophysical source rather than from noise in the detector. The document summarizes the differences between the ranking routines of each search pipeline. The goal is to understand their respective efficiency for subsolar mass black hole binaries search. This document has been sent to the PBH-DM group of the LIGO-Virgo-KAGRA collaboration and will be supplemented by new updates from the pipeline teams. Link to the document:

https://docs.google.com/document/d/1bwAiRNKh1jYasH_USl4SLksHuicg2Co7sWs1lj3FAyY/edit?usp=sharing

B Parameter Estimation results for SSMC2

A similar analysis to the one performed with SSMC1 was made for SSMC2, the results are summarized in the Table 4 and in Figures 15, 16 and 17.

Masses In Figure 15 is shown the posterior distribution of the SSMC2's component masses (the prior on these masses was uniform between 0.1 and 2 solar mass). SSMC2's source corresponds to a subsolar-mass event with individual source-frame masse $m_1 = 1.05^{+0.40}_{-0.22}$ $M_\odot$ and $m_2 = 0.57^{+0.14}_{-0.13}$ $M_\odot$. The two compact objects are not of equal mass, their mass ratio $q = \frac{m_2}{m_1}$ is bound to the range $0.30 \leq q \leq 0.85$. These component masses were computed using the chirp mass M_c and the mass ratio q (Fig.15. The chirp mass posterior is tightly constrained with $M_c = 0.67^{+0.01}_{-0.01}$. The parameter estimation results on the component masses of SSMC2 show the subsolar origin of the second binary component with great certainty. The first binary component has $P(m_1 \leq 1M_\odot) = 45\%$ and $P(m_1 \leq 1.2M_\odot) = 59\%$ could be classified as a subsolar-mass black hole or a light neutron star. The second mass has 100 % of being subsolar according to the PE results.

Distance and orientation The luminosity distance d_L and inclination angle θ_{JN} posterior distributions are shown together in Figure 16, with d_L given in Mpc and θ_{JN} in radians. The corner plot shows a clear bimodal distribution for θ_{JN} due to the fact that one can not distinguish whether the system is being observed face-on ($\theta_{JN} \sim 0$) or face-away ($\theta_{JN} \sim \pi$), nevertheless the system being edge-on ($\theta_{JN} \sim \pi/2$) seem disfavoured.

The posterior distribution for the redshift of the source; $z = 0.04^{+0.01}_{-0.02}$

Spins χ_{eff} is a conserved quantity throughout the inspiral phase of the merger, it is a dimensionless number ranging from -1 to 1, where if $\chi_{eff} = 1$ the spins of the compact objects are aligned with their orbit, and if χ_{eff} = -1 the spins are perfectly anti-aligned. $\chi_{eff} \sim 0$ can mean that the magnitude of the spin parameters is $\ll 1$ or indicates a formation channel where spins are largely uncorrelated with their orbit (which is the case for PBHs [34], plus are predicted to have small intrinsic spins). SSMC2 seems to have a $\chi_{eff} \sim 0$, which is coherent with a PBH origin scenario. In Figure 16 is plotted χ_{eff} along with the effective precession spin parameter, χ_p ($\chi_p \sim 0$ would indicate no spin precession of the orbital plane and a value of $\chi_p = 1$ a maximal precession). The posterior of χ_p is not very informative with a broad confidence interval.

Parameter	Values
Primary mass ($M_\odot$)	$1.05^{+0.40}_{-0.22}$
Secondary mass ($M_\odot$)	$0.57^{+0.14}_{-0.13}$
Final mass ($M_\odot$)	$1.62^{+0.27}_{-0.09}$
Mass ratio ($m_2/m_1 < 1$)	$0.54^{+0.31}_{-0.24}$
Chirp Mass	$0.67^{+0.01}_{-0.01}$
χ_{eff}	$-0.05^{+0.24}_{-0.32}$
χ_p	$0.44^{+0.28}_{-0.23}$
Luminosity Distance (Mpc)	$199.18^{+64.19}_{-70.82}$
Redshift	$0.04^{+0.02}_{-0.01}$
Global SNR	10.09
P($m_1 < 1\ M_\odot$)	45%
P($m_2 < 1\ M_\odot$)	100%

Table 4: Results of the parameter estimation for SSMC2. All masses are in the source frame. The statistical uncertainty of all the parameters is quantified by the 68% credible intervals about the median of the marginalized one-dimensional posteriors.

Bayes Factor For the SSMC2 candidate, I obtain $\log(B_{S,N}) = 0.43$. This result shows a slight preference for the *signal model* but can not discard the *noise hypothesis*.

Bayes Coherence Ratio (BCR) For the SSMC2 candidate, I obtain $\log(BCR) = 0.02$. This result does not allow us to draw a firm conclusion on the coherence or incoherence of the signal.

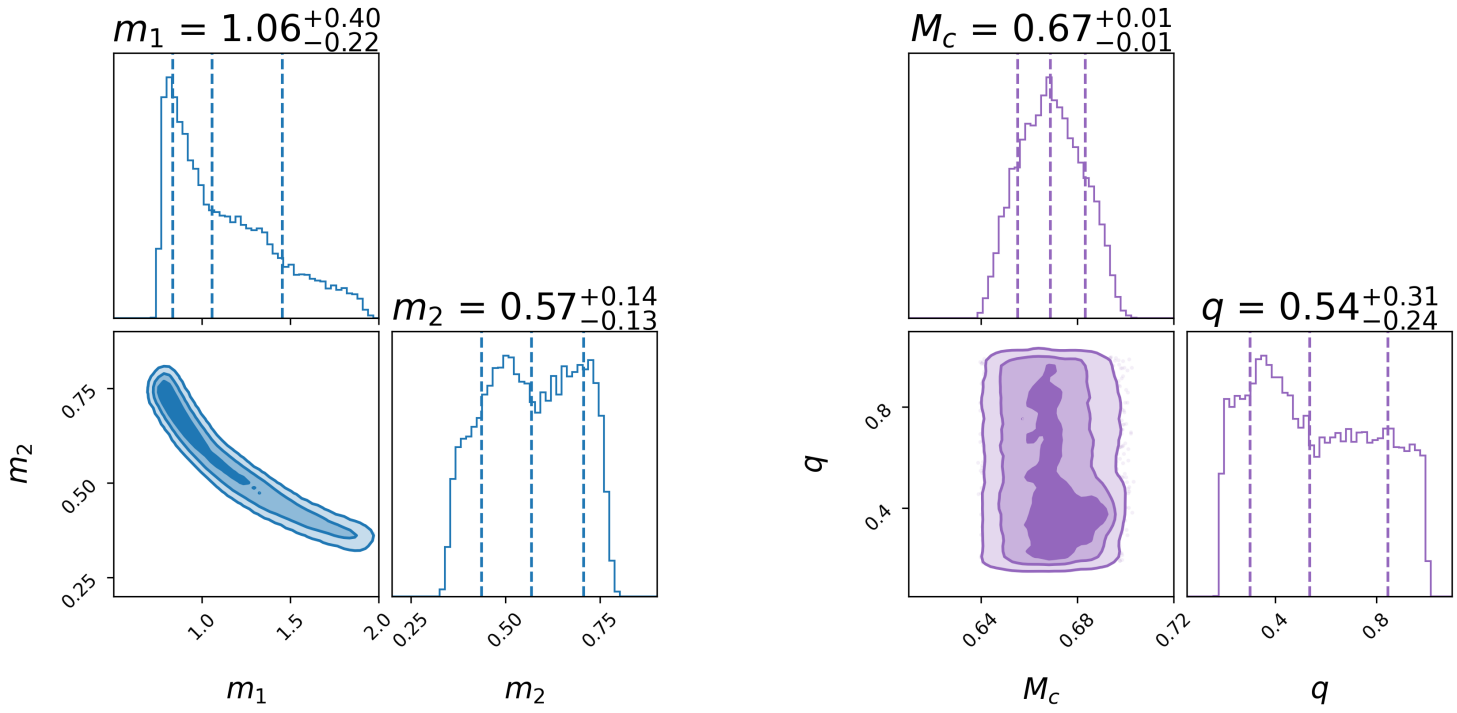

Figure 15: Left: Corner plot for the black hole masses. For each parameter is reported the median value and 1-sigma error. The contours of the 2D histogram correspond to the range of the symmetric 39%, 86%, and 99% credible interval with respect to the median. **Right:** Corner plot for the chirp mass and mass ratio.

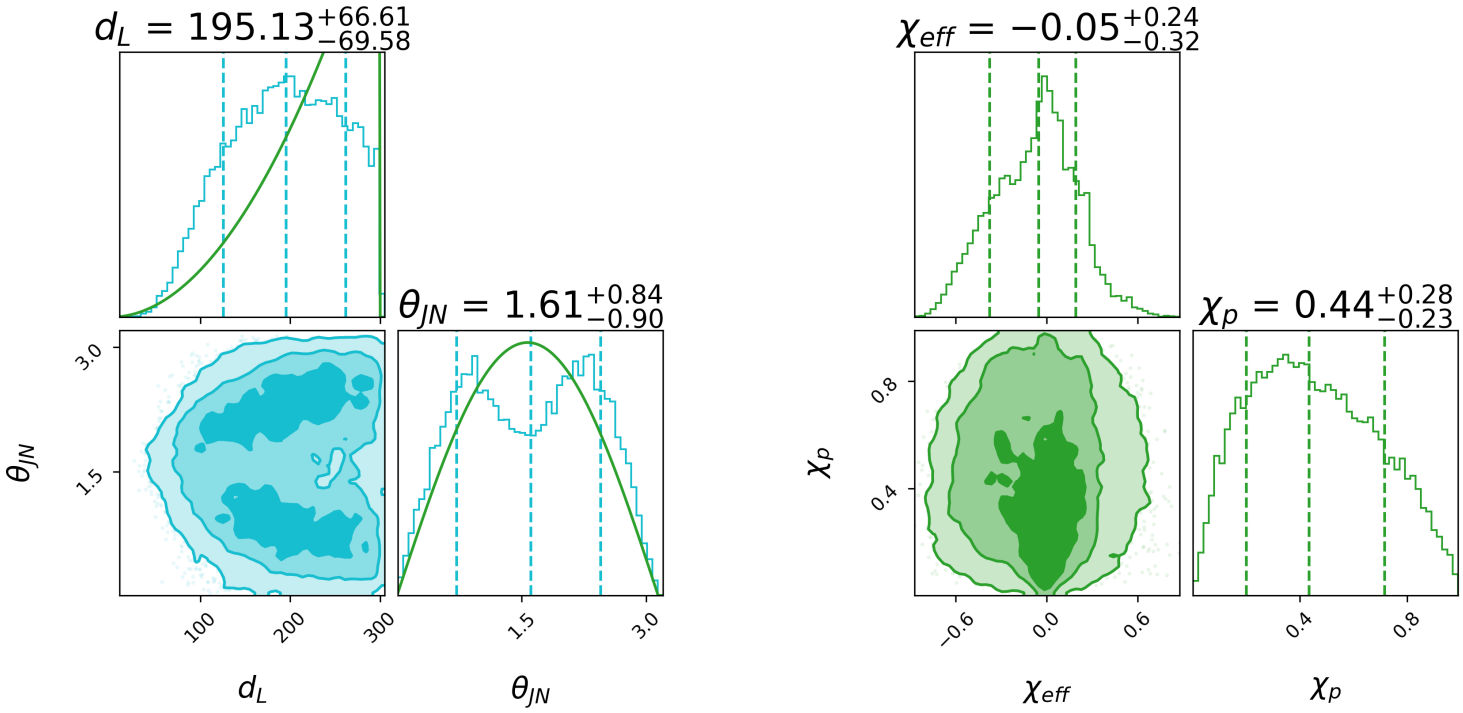

Figure 16: Left: Corner plot for the luminosity distance and θ_{JN}. Priors are shown in green. **Right:** Corner plot for χ_{eff} and χ_p.

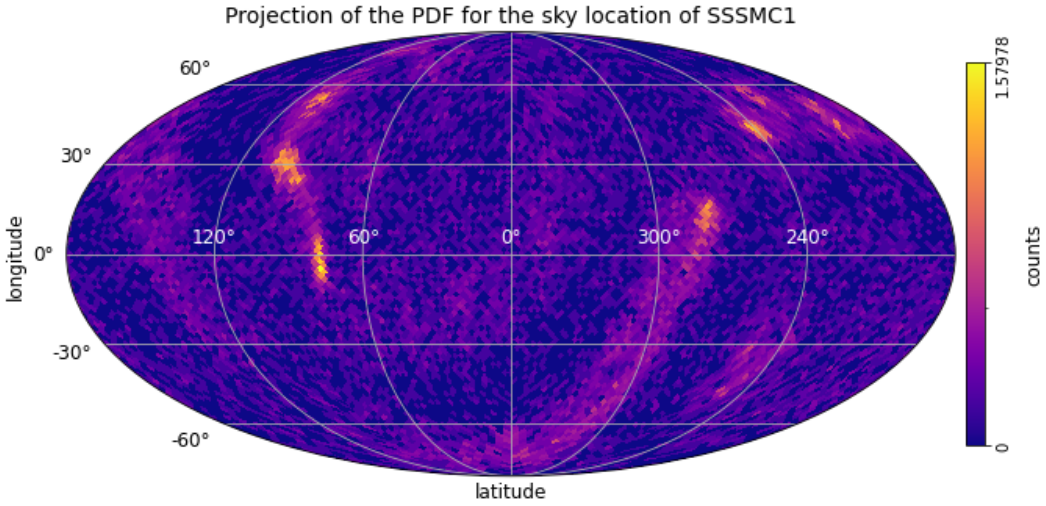

Figure 17: Posterior of the sky location of the SSMC2 source in Galactic Coordinate (with the Galactic center in the middle).

C Nested Sampling Theory

Nested Sampling is designed to compute the evidence $Z(\mathbf{d}|H)$. This evidence, which is the normalization factor in the Bayes formula, corresponds to the integral over the entire parameter space. The key idea of Nested Sampling is that this high-dimension problem can be ingeniously mapped into an easier 1D integration problem. If we define the prior volume X, and the total probability volume contained within a likelihood contour defined by $p(\mathbf{d}|\vec{\theta}, H) = \lambda$:

$$X(\lambda) = \int_{dX>\lambda} dX = \int_{p(d|\theta,M)>\lambda} d\vec{\theta}\, p(\vec{\theta}|M) \tag{22}$$

Then we can rewrite the multi dimensional eq.22 as follow this 1D integral [29]:

$$Z = \int_0^1 dX L(X) \tag{23}$$

By evaluating the likelihoods L_i associated with a monotonically decreasing sequence of prior volumes X_i:

$$0 < X_M < .... < X_2 < X_1 < 1 \tag{24}$$

and Z can be approximated with numerical integration (trapezium rule for example) :

$$Z = \frac{1}{2}(X_{i+1} - X_{i-1})L_i = \sum_{i=1}^{M} \Delta V_i L_i \tag{25}$$

How does Nested Sampling computes Z in practice?
Let's consider that we want to compute the marginal likelihood over a 2-dimensional continuous parameter space $\vec{\theta} = \{\theta_1, \theta_2\}$, the Nested Sampling algorithm goes as follows:

- **Initialisation :** We sample N live points from the prior parameter space (see Fig.18).
- **Shrinkage :** Find and remove the live point having the worst likelihood L^*, which becomes the first *dead point*. This removal reduces the prior volume by a factor shell ΔV_i corresponding to the prior volume inside the current iso-likelihood contour line; $\Delta V_i \sim e^{-1/N} \times V_i$ where V_i is the prior volume at this stage (Fig.19).

- **Likelihood-restricted prior sampling (LRPS)** A new, independent live point with $L > L^*$ is sampled from the prior. **How ?** The algorithm uses one of the other points to initialize a quick MCMC run, trying to sample the prior, but rejecting any proposal with likelihood below L^*.

- **Termination** Repeat replacing live points (shrinking and LRPS steps), which continuously increases the likelihood threshold and shrinks the volume by approximately a constant volume fraction. When the likelihood variation of the remaining live points tends to zero (Fig.20), contributions to Z are thus negligible and the integration can be stopped.

- **Evidence computation :** At each step, we save the live point with the lowest likelihood (*the dead point*) as a sample point with weight $w_i = \Delta V_i \cdot L_i$. The integral Z is simply: $Z \sim \sum_i \Delta V_i \cdot L_i$.

- **Posterior samples** When Z is estimated the posterior sample can be obtained by resampling the chain of *dead points* and current live points according to their posterior probabilities. Indeed, as the nested sampling algorithm proceeds, the list of points used to approximate the evidence is stored along with the associated likelihood L_i and weight ΔV_i :

$$p(\theta_i|d, H) = \frac{\Delta V_i \cdot L_i}{Z} \tag{26}$$

  Therefore it is easy to obtain the marginalized posterior by histogramming the samples (as can be seen in Fig.20.

The following figures illustrate the different steps of the Nested Sampling Algorithm computing the evidence of a 2-D likelihood function and the posterior distribution of θ_1.

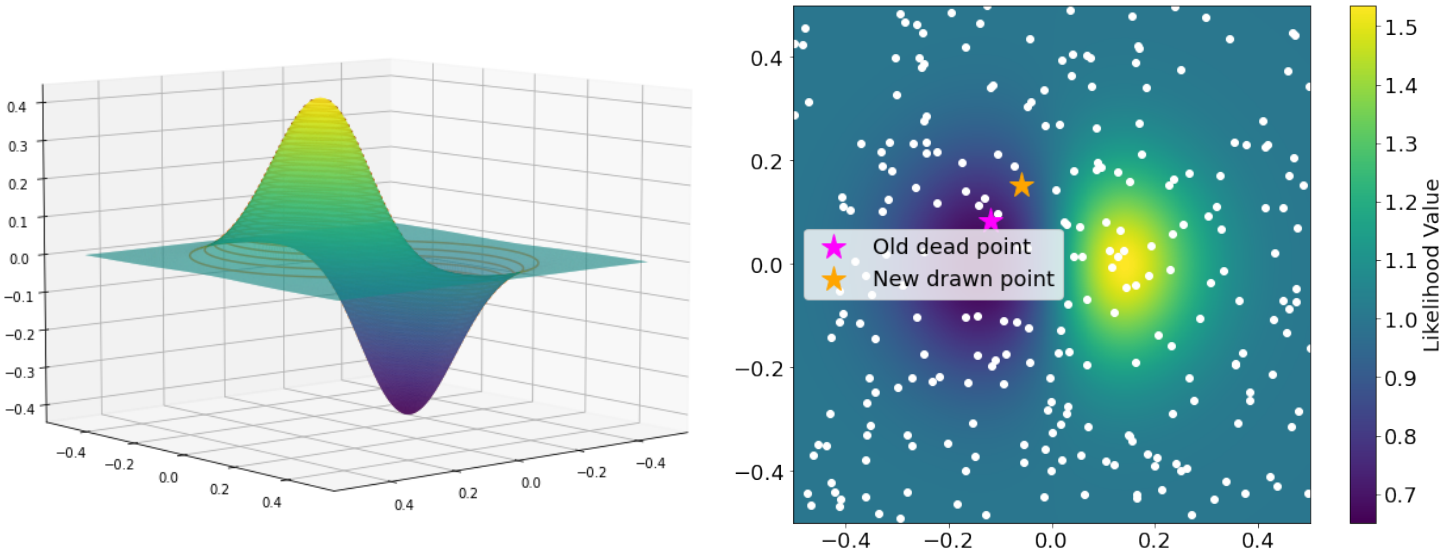

Figure 18: Left: We have this 2D target function (likelihood x prior) and we want to compute its evidence (integrate it). **Right:** First N sampled live points on the prior parameter space. The one having the lowest likelihood value goes to the dead points. A new live point with better likelihood is drawn.

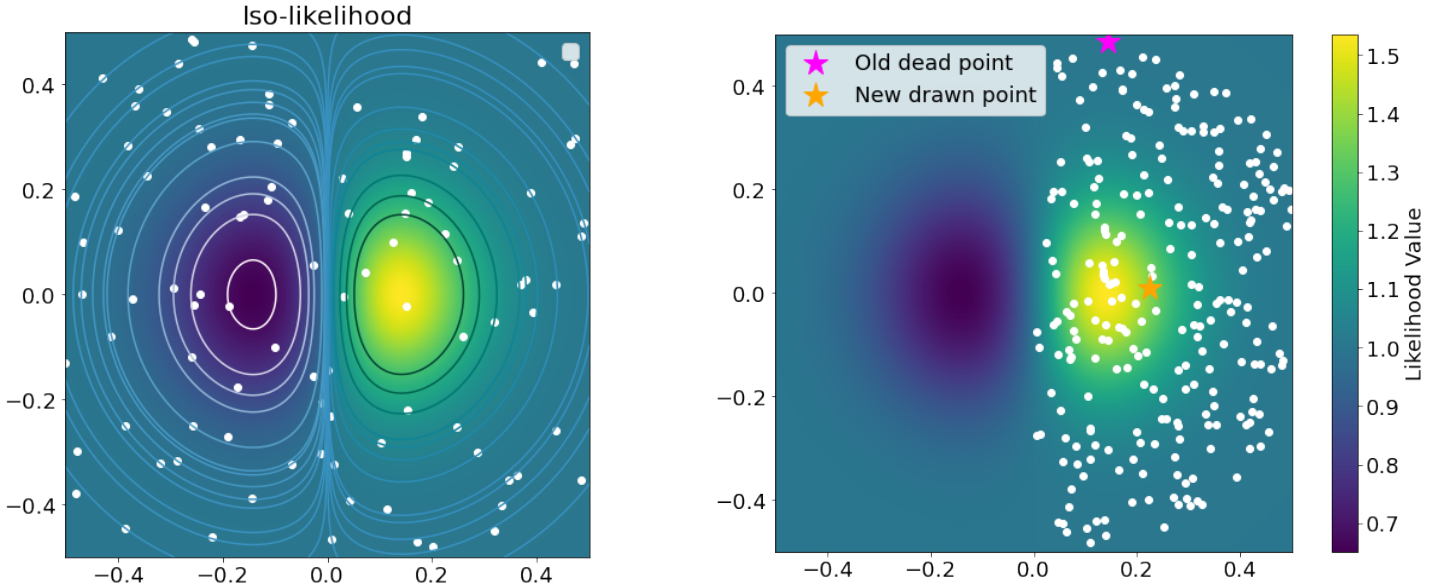

Figure 19: Left: Iso-Likelihood contour associated with each live point. In between lies approximately similar prior volume, the fractions are distributed as $\sim e^{-1/N}$. When a dead point is removed, the prior volume is reduced by ΔV between the closest iso-likelihood. **Right:** After a few iterations. The prior volume has been shrunk.

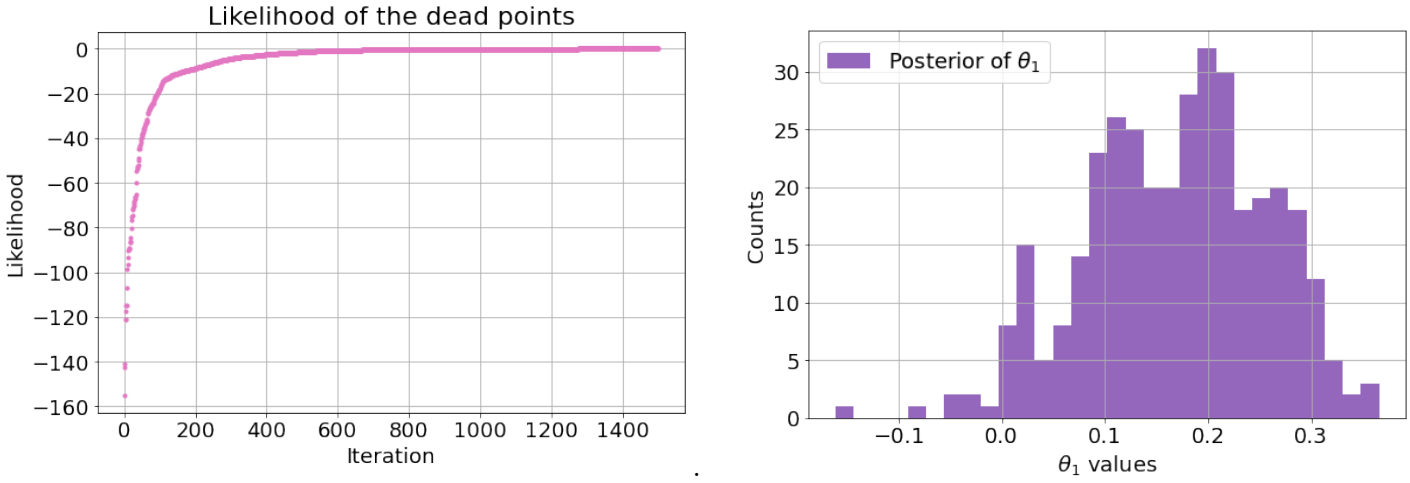

Figure 20: Left: Termination when the likelihood of the dead points becomes flat. **Right:** Posterior distribution of the θ_1 parameter.

D Signal-to-noise ratio of a gravitational wave signal

In general, we assume the noise of the detectors to be an uncorrelated Gaussian noise with zero mean $\langle \tilde{n} \rangle = 0$ and stationary meaning that the different Fourier modes are uncorrelated:

$$\langle \tilde{n}^*(f)\tilde{n}(f')\rangle = \frac{1}{2}S_n(f)\delta(f-f') \tag{27}$$

This is the standard definition of the noise power spectral density (PSD) $S_n(f)$. Using this PSD we can define the **optimal SNR**, corresponding to the SNR when the template h_T for the gravitational waveform of the signal is identical to the real GW waveform h (ideal case):

$$SNR_{opt} = \sqrt{\langle h, h\rangle} \tag{28}$$

The inner product is defined as (tilde denotes the Fourier transforms):

$$\langle a, b\rangle = 4Re\int_{f_{min}}^{f_{max}} \frac{\tilde{a}^*(f)\tilde{b}(f)}{S_n(f)}\, df \tag{29}$$

And the **matched filter** SNR :

$$SNR_{mf} = \frac{\langle h, d\rangle}{SNR_{opt}} \tag{30}$$

where d is the detector strain data. Given the template h and the PSD $S_n(f)$ of the data for a GW signal, one can compute the loss of SNR compared to the optimal SNR when starting the analysis at $f_{start} > f_{min}$. This is what is shown in Fig. 10 (Right panel) for the candidate SSMC1.

E Choice of parametrization

The GW signal received by the detectors is dominated by several cycles of a wave pattern whose amplitude is initially increasing. A useful quantity for assessing the sensitivity of the detectors to inspiraling binaries is the number of cycles spent in the detector bandwidth $[f_{min}, f_{max}]$. When the period $T(t)$ of the GW is a slowly varying function of time, the number of cycles in time interval dt is given by:

$$dN_{cycles} = dt/T(t) = f_{gw}(t)dt \tag{31}$$

so

$$N_{cycles} = \int f_{gw}(t)dt \tag{32}$$

and with the definition of $\dot{f}_{gw}$ from the literature we obtain:

$$N_{cycles} = \frac{1}{32\pi^{3/8}} \left(\frac{GM_c}{c^3}\right)^{-5/3} (f_{min}^{-5/3} - f_{max}^{-5/3}) \tag{33}$$

$$N_{cycles} = 1.8 \cdot 10^4 \left(\frac{40\text{Hz}}{f_{min}}\right)^{5/3} \left(\frac{0.35M_\odot}{M_c}\right)^{5/3} \tag{34}$$

The chirp mass appears in the waveform phase term, which phase can be estimated very precisely since the phase can be followed accurately for N_{cycles} cycles. Any mismatch ΔM_c between the true value of the source and the value used in the template will be amplified by a factor N_{cycles}: $\frac{\Delta M_c}{M_c} \sim \frac{1}{N_{cycles}}$ [24].

F `BILBY` implementation

Parameters used to initiate the Nested Sampling algorithm with `BILBY` :

Sampler	`dynesty`
Live Points	600
naccept	60
dlogz	0.1
Duration [sec]	130
npool	16
Sampling frequency [Hz]	4096
Minimum frequency [Hz]	50
Maximum frequency [Hz]	1800
Waveform Approximant	`IMRPhenomPv2`
Reference frequency [Hz]	100
Calibration Marginalization	False
Distance Marginalization	True
Phase Marginalization	True
Time Marginalization	True

Table 5

I use `Bilby Pipe` on the LIGO Hanford Computing Cluster (node `ldas-pcdev1.ligo-wa.caltech`). In the script, setting `coherence-test` to `True` performs the parameter estimation for each detector separately in addition to the default joint one. This mode computes the evidence for each detector Z_i and allows to calculate the BCR. **The codes and results are all available on** my github.

Bibliography

[1] LIGO Scientific Collaboration and Virgo Collaboration. "Observation of Gravitational Waves from a Binary Black Hole Merger". In: *Physical Review Letters* 116.6 (Feb. 2016). Publisher: American Physical Society, p. 061102. DOI: 10.1103/PhysRevLett.116.061102. URL: https://link.aps.org/doi/10.1103/PhysRevLett.116.061102 (visited on 05/22/2023).

[2] The LIGO Scientific Collaboration, the Virgo Collaboration, and the KAGRA Collaboration. *GWTC-3: Compact Binary Coalescences Observed by LIGO and Virgo During the Second Part of the Third Observing Run*. Tech. rep. Publication Title: arXiv e-prints ADS Bibcode: 2021arXiv211103606T Type: article. Nov. 2021. DOI: 10.48550/arXiv.2111.03606. URL: https://ui.adsabs.harvard.edu/abs/2021arXiv211103606T (visited on 06/09/2023).

[3] Simeon Bird et al. "Did LIGO detect dark matter?" In: *Physical Review Letters* 116.20 (May 2016). arXiv:1603.00464 [astro-ph, physics:hep-ph], p. 201301. ISSN: 0031-9007, 1079-7114. DOI: 10.1103/PhysRevLett.116.201301. URL: http://arxiv.org/abs/1603.00464 (visited on 05/14/2023).

[4] Misao Sasaki et al. "Primordial Black Hole Scenario for the Gravitational-Wave Event GW150914". In: *Physical Review Letters* 117.6 (Aug. 2016). arXiv:1603.08338 [astro-ph, physics:gr-qc], p. 061101. ISSN: 0031-9007, 1079-7114. DOI: 10.1103/PhysRevLett.117.061101. URL: http://arxiv.org/abs/1603.08338 (visited on 05/14/2023).

[5] Sebastien Clesse and Juan García-Bellido. "The clustering of massive Primordial Black Holes as Dark Matter: measuring their mass distribution with Advanced LIGO". In: *Physics of the Dark Universe* 15 (Mar. 2017). arXiv:1603.05234 [astro-ph, physics:hep-th], pp. 142–147. ISSN: 22126864. DOI: 10.1016/j.dark.2016.10.002. URL: http://arxiv.org/abs/1603.05234 (visited on 05/02/2023).

[6] Giorgio Arcadi et al. "The Waning of the WIMP? A Review of Models, Searches, and Constraints". In: *The European Physical Journal C* 78.3 (Mar. 2018). arXiv:1703.07364 [astro-ph, physics:hep-ex, physics:hep-ph, physics:hep-th], p. 203. ISSN: 1434-6044, 1434-6052. DOI: 10.1140/epjc/s10052-018-5662-y. URL: http://arxiv.org/abs/1703.07364 (visited on 05/22/2023).

[7] B. P. Abbott, R. Abbott, and et al. Abbott. "Search for sub-solar mass ultracompact binaries in Advanced LIGO's first observing run". In: *Physical Review Letters* 121.23 (Dec. 2018). arXiv:1808.04771 [astro-ph, physics:gr-qc], p. 231103. ISSN: 0031-9007, 1079-7114. DOI: 10.1103/PhysRevLett.121.231103. URL: http://arxiv.org/abs/1808.04771 (visited on 05/02/2023).

[8] LIGO Scientific Collaboration and the Virgo Collaboration. "Search for Subsolar Mass Ultracompact Binaries in Advanced LIGO's Second Observing Run". In: *Physical Review Letters* 123.16 (Oct. 2019). Publisher: American Physical Society, p. 161102. DOI: 10.1103/PhysRevLett.123.161102. URL: https://link.aps.org/doi/10.1103/PhysRevLett.123.161102 (visited on 05/05/2023).

[9] Khun Sang Phukon et al. *The hunt for sub-solar primordial black holes in low mass ratio binaries is open*. arXiv:2105.11449 [astro-ph, physics:gr-qc, physics:hep-th]. May 2021. DOI: 10.48550/arXiv.2105.11449. URL: http://arxiv.org/abs/2105.11449 (visited on 05/02/2023).

[10] Gonzalo Morrás et al. *Analysis of a subsolar-mass black hole trigger from the second observing run of Advanced LIGO*. arXiv:2301.11619 [astro-ph, physics:gr-qc]. Jan. 2023. URL: http://arxiv.org/abs/2301.11619 (visited on 06/08/2023).

[11] Alexander H. Nitz and Yi-Fan Wang. "Broad search for gravitational waves from subsolar-mass binaries through LIGO and Virgo's third observing run". In: *Physical Review D* 106.2 (July 2022). Publisher: American Physical Society, p. 023024. DOI: 10.1103/PhysRevD.106.023024. URL: https://link.aps.org/doi/10.1103/PhysRevD.106.023024 (visited on 05/05/2023).

[12] Alexander H. Nitz and Yi-Fan Wang. "Search for Gravitational Waves from the Coalescence of Subsolar-Mass Binaries in the First Half of Advanced LIGO and Virgo's Third Observing Run". In: *Physical Review Letters* 127.15 (Oct. 2021). Publisher: American Physical Society, p. 151101. DOI: 10.1103/PhysRevLett.127.151101. URL: https://link.aps.org/doi/10.1103/PhysRevLett.127.151101 (visited on 05/05/2023).

[13] The LIGO Scientific Collaboration, the Virgo Collaboration, and the KAGRA Collaboration. *Search for subsolar-mass black hole binaries in the second part of Advanced LIGO's and Advanced Virgo's third observing run*. arXiv:2212.01477 [astro-ph]. Dec. 2022. URL: http://arxiv.org/abs/2212.01477 (visited on 06/06/2023).

[14] Kipp Cannon et al. "GstLAL: A software framework for gravitational wave discovery". en. In: *SoftwareX* 14 (June 2021), p. 100680. ISSN: 2352-7110. DOI: 10.1016/j.softx.2021.100680. URL: https://www.sciencedirect.com/science/article/pii/S235271102100025X (visited on 05/22/2023).

[15] Florian Aubin et al. "The MBTA Pipeline for Detecting Compact Binary Coalescences in the Third LIGO-Virgo Observing Run". In: *Classical and Quantum Gravity* 38.9 (May 2021). arXiv:2012.11512 [gr-qc], p. 095004. ISSN: 0264-9381, 1361-6382. DOI: 10.1088/1361-6382/abe913. URL: http://arxiv.org/abs/2012.11512 (visited on 05/22/2023).

[16] C. M. Biwer et al. "PyCBC Inference: A Python-based parameter estimation toolkit for compact binary coalescence signals". In: *Publ. Astron. Soc. Pac.* 131.996 (2019). DOI: 10.1088/1538-3873/aaef0b. arXiv: 1807.10312 [astro-ph.IM].

[17] Ya. B. Zel'dovich and I. D. Novikov. "The Hypothesis of Cores Retarded during Expansion and the Hot Cosmological Model". In: *Soviet Astronomy* 10 (Feb. 1967). ADS Bibcode: 1967SvA....10..602Z, p. 602. ISSN: 0038-5301. URL: https://ui.adsabs.harvard.edu/abs/1967SvA....10..602Z (visited on 05/03/2023).

[18] Stephen Hawking. "Gravitationally collapsed objects of very low mass". In: *Monthly Notices of the Royal Astronomical Society* 152 (Jan. 1971). ADS Bibcode: 1971MNRAS.152...75H, p. 75. ISSN: 0035-8711. DOI: 10.1093/mnras/152.1.75. URL: https://ui.adsabs.harvard.edu/abs/1971MNRAS.152...75H (visited on 05/02/2023).

[19] Planck Collaboration. "Planck 2015 results. XIII. Cosmological parameters". In: *Astronomy & Astrophysics* 594 (Oct. 2016). arXiv:1502.01589 [astro-ph], A13. ISSN: 0004-6361, 1432-0746. DOI: 10.1051/0004-6361/201525830. URL: http://arxiv.org/abs/1502.01589 (visited on 05/22/2023).

[20] S. W. Hawking. "Particle Creation by Black Holes". In: *Commun. Math. Phys.* 43 (1975). Ed. by G. W. Gibbons and S. W. Hawking, pp. 199–220. DOI: 10.1007/BF02345020.

[21] Pablo Villanueva-Domingo, Olga Mena, and Sergio Palomares-Ruiz. "A Brief Review on Primordial Black Holes as Dark Matter". In: *Frontiers in Astronomy and Space Sciences* 8 (2021). ISSN: 2296-987X. URL: https://www.frontiersin.org/articles/10.3389/fspas.2021.681084 (visited on 05/03/2023).

[22] Bernard Carr et al. "Constraints on Primordial Black Holes". In: *Reports on Progress in Physics* 84.11 (Nov. 2021). arXiv:2002.12778 [astro-ph, physics:gr-qc, physics:hep-ph, physics:hep-th], p. 116902. ISSN: 0034-4885, 1361-6633. DOI: 10.1088/1361-6633/ac1e31. URL: http://arxiv.org/abs/2002.12778 (visited on 05/02/2023).

[23] Bernard Carr et al. "Observational Evidence for Primordial Black Holes: A Positivist Perspective". In: (June 2023). arXiv: 2306.03903 [astro-ph.CO].

[24] Sascha Husa. "Michele Maggiore: Gravitational waves. Volume 1: theory and experiments". en. In: *General Relativity and Gravitation* 41.7 (July 2009), pp. 1667–1669. ISSN: 1572-9532. DOI: 10.1007/s10714-009-0762-5. URL: https://doi.org/10.1007/s10714-009-0762-5 (visited on 05/02/2023).

[25] G. L. Turin. "An introduction to matched filters". In: *IRE Transactions on Information Theory* (1960).

[26] Leah Vazsonyi and Derek Davis. "Identifying glitches near gravitational-wave signals from compact binary coalescences using the Q-transform". In: *Classical and Quantum Gravity* 40.3 (Feb. 2023). arXiv:2208.12338 [astro-ph, physics:gr-qc], p. 035008. ISSN: 0264-9381, 1361-6382. DOI: 10.1088/1361-6382/acafd2. URL: http://arxiv.org/abs/2208.12338 (visited on 05/14/2023).

[27] Neil J. Cornish and Tyson B. Littenberg. "BayesWave: Bayesian Inference for Gravitational Wave Bursts and Instrument Glitches". In: *Classical and Quantum Gravity* 32.13 (July 2015). arXiv:1410.3835 [astro-ph, physics:gr-qc], p. 135012. ISSN: 0264-9381, 1361-6382. DOI: 10.1088/0264-9381/32/13/135012. URL: http://arxiv.org/abs/1410.3835 (visited on 05/14/2023).

[28] Chris Pankow et al. "Mitigation of the instrumental noise transient in gravitational-wave data surrounding GW170817". In: *Physical Review D* 98.8 (Oct. 2018). arXiv:1808.03619 [gr-qc], p. 084016. ISSN: 2470-0010, 2470-0029. DOI: 10.1103/PhysRevD.98.084016. URL: http://arxiv.org/abs/1808.03619 (visited on 05/14/2023).

[29] John Skilling. "Nested Sampling". In: 735 (Nov. 2004). Conference Name: Bayesian Inference and Maximum Entropy Methods in Science and Engineering: 24th International Workshop on Bayesian Inference and Maximum Entropy Methods in Science and Engineering ADS Bibcode: 2004AIPC..735..395S, pp. 395–405. DOI: 10.1063/1.1835238. URL: https://ui.adsabs.harvard.edu/abs/2004AIPC..735..395S (visited on 05/26/2023).

[30] LIGO Scientific Collaboration. *LIGO Algorithm Library - LALSuite*. free software (GPL). 2018. DOI: 10.7935/GT1W-FZ16.

[31] Gregory Ashton et al. "Bilby: A user-friendly Bayesian inference library for gravitational-wave astronomy". In: *The Astrophysical Journal Supplement Series* 241.2 (Apr. 2019). arXiv:1811.02042 [astro-ph, physics:gr-qc], p. 27. ISSN: 1538-4365. DOI: 10.3847/1538-4365/ab06fc. URL: http://arxiv.org/abs/1811.02042 (visited on 06/06/2023).

[32] P. Welch. "The use of fast Fourier transform for the estimation of power spectra: A method based on time averaging over short, modified periodograms". In: *IEEE Transactions on Audio and Electroacoustics* 15.2 (1967), pp. 70–73. DOI: 10.1109/TAU.1967.1161901.

[33] Enrico Barausse, Sabino Matarrese, and Antonio Riotto. "The Effect of Inhomogeneities on the Luminosity Distance-Redshift Relation: is Dark Energy Necessary in a Perturbed Universe?" In: *Physical Review D* 71.6 (Mar. 2005). arXiv:astro-ph/0501152, p. 063537. ISSN: 1550-7998, 1550-2368. DOI: 10.1103/PhysRevD.71.063537. URL: http://arxiv.org/abs/astro-ph/0501152 (visited on 06/20/2023).

[34] Nicolas Fernandez and Stefano Profumo. "Unraveling the origin of black holes from effective spin measurements with LIGO-Virgo". In: *Journal of Cosmology and Astroparticle Physics* 2019.08 (Aug. 2019). arXiv:1905.13019 [astro-ph, physics:gr-qc, physics:hep-ph], pp. 022–022. ISSN: 1475-7516. DOI: 10.1088/1475-7516/2019/08/022. URL: http://arxiv.org/abs/1905.13019 (visited on 05/31/2023).

[35] Eric Thrane and Colm Talbot. "An introduction to Bayesian inference in gravitational-wave astronomy: parameter estimation, model selection, and hierarchical models". In: *Publications of the Astronomical Society of Australia* 36 (2019). arXiv:1809.02293 [astro-ph], e010. ISSN: 1323-3580, 1448-6083. DOI: 10.1017/pasa.2019.2. URL: http://arxiv.org/abs/1809.02293 (visited on 06/09/2023).

[36] Eric Thrane and Colm Talbot. "An introduction to Bayesian inference in gravitational-wave astronomy: Parameter estimation, model selection, and hierarchical models". In: *Publications of the Astronomical Society of Australia* 36 (2019), e010. DOI: 10.1017/pasa.2019.2.

[37] John Veitch and Alberto Vecchio. "Bayesian coherent analysis of in-spiral gravitational wave signals with a detector network". In: *Physical Review D* 81.6 (Mar. 2010). arXiv:0911.3820 [astro-ph, physics:gr-qc, physics:physics], p. 062003. ISSN: 1550-7998, 1550-2368. DOI: 10.1103/PhysRevD.81.062003. URL: http://arxiv.org/abs/0911.3820 (visited on 05/31/2023).

[38] John Veitch et al. "Robust parameter estimation for compact binaries with ground-based gravitational-wave observations using the LALInference software library". In: *Physical Review D* 91.4 (Feb. 2015). arXiv:1409.7215 [astro-ph, physics:gr-qc], p. 042003. ISSN: 1550-7998, 1550-2368. DOI: 10.1103/PhysRevD.91.042003. URL: http://arxiv.org/abs/1409.7215 (visited on 05/02/2023).

[39] Maximiliano Isi et al. "Enhancing confidence in the detection of gravitational waves from compact binaries using signal coherence". In: *Physical Review D* 98.4 (Aug. 2018). arXiv:1803.09783 [astro-ph, physics:gr-qc, physics:physics], p. 042007. ISSN: 2470-0010, 2470-0029. DOI: 10.1103/PhysRevD.98.042007. URL: http://arxiv.org/abs/1803.09783 (visited on 05/31/2023).

[40] Walter del Pozzo et al. "Testing general relativity with compact coalescing binaries: comparing exact and predictive methods to compute the Bayes factor". In: *Classical and Quantum Gravity* 31 (2014).

[41] James M. Lattimer. "Neutron Star Mass and Radius Measurements". In: *Universe* 5.7 (2019), p. 159. DOI: 10.3390/universe5070159.

[42] J. M. Lattimer and M. Prakash. "Neutron Star Structure and the Equation of State". en. In: *The Astrophysical Journal* 550.1 (Mar. 2001). Publisher: IOP Publishing, p. 426. ISSN: 0004-637X. DOI: 10.1086/319702. URL: https://iopscience.iop.org/article/10.1086/319702/meta (visited on 05/31/2023).

[43] The LIGO Scientific Collaboration and The Virgo Collaboration. "GW170817: Observation of Gravitational Waves from a Binary Neutron Star Inspiral". In: *Physical Review Letters* 119.16 (Oct. 2017). arXiv:1710.05832 [astro-ph, physics:gr-qc], p. 161101. ISSN: 0031-9007, 1079-7114. DOI: 10.1103/PhysRevLett.119.161101. URL: http://arxiv.org/abs/1710.05832 (visited on 05/02/2023).

[44] Adam Burrows et al. "The Overarching Framework of Core-Collapse Supernova Explosions as Revealed by 3D Fornax Simulations". In: *Monthly Notices of the Royal Astronomical Society* 491.2 (Jan. 2020). arXiv:1909.04152 [astro-ph], pp. 2715–2735. ISSN: 0035-8711, 1365-2966. DOI: 10.1093/mnras/stz3223. URL: http://arxiv.org/abs/1909.04152 (visited on 05/31/2023).

[45] B. Müller et al. "Three-Dimensional Simulations of Neutrino-Driven Core-Collapse Supernovae from Low-Mass Single and Binary Star Progenitors". In: *Monthly Notices of the Royal Astronomical Society* 484.3 (Apr. 2019). arXiv:1811.05483 [astro-ph], pp. 3307–3324. ISSN: 0035-8711, 1365-2966. DOI: 10.1093/mnras/stz216. URL: http://arxiv.org/abs/1811.05483 (visited on 05/31/2023).

[46] B P Abbott, R Abbott, and Abbott et al. "Model comparison from LIGO–Virgo data on GW170817's binary components and consequences for the merger remnant". In: *Classical and Quantum Gravity* 37.4 (Feb. 2020), p. 045006. ISSN: 0264-9381, 1361-6382. DOI: 10.1088/1361-6382/ab5f7c. URL: https://iopscience.iop.org/article/10.1088/1361-6382/ab5f7c (visited on 06/09/2023).

[47] S. Blinnikov et al. "Solving puzzles of GW150914 by primordial black holes". In: *Journal of Cosmology and Astroparticle Physics* 2016.11 (Nov. 2016). arXiv:1611.00541 [astro-ph], pp. 036–036. ISSN: 1475-7516. DOI: 10.1088/1475-7516/2016/11/036. URL: http://arxiv.org/abs/1611.00541 (visited on 05/14/2023).

[48] Maya Fishbach and Vicky Kalogera. "Apples and Oranges: Comparing black holes in X-ray binaries and gravitational-wave sources". In: *The Astrophysical Journal Letters* 929.2 (Apr. 2022). arXiv:2111.02935 [astro-ph, physics:gr-qc], p. L26. ISSN: 2041-8205, 2041-8213. DOI: 10.3847/2041-8213/ac64a5. URL: http://arxiv.org/abs/2111.02935 (visited on 05/14/2023).

[49] S. E. Woosley and Alexander Heger. "The Pair-instability Mass Gap for Black Holes". en. In: *The Astrophysical Journal Letters* 912.2 (May 2021). Publisher: The American Astronomical Society, p. L31. ISSN: 2041-8205. DOI: 10.3847/2041-8213/abf2c4. URL: https://dx.doi.org/10.3847/2041-8213/abf2c4 (visited on 05/31/2023).

[50] R. Farmer et al. "Mind the gap: The location of the lower edge of the pair instability supernovae black hole mass gap". In: *The Astrophysical Journal* 887.1 (Dec. 2019). arXiv:1910.12874 [astro-ph], p. 53. ISSN: 1538-4357. DOI: 10.3847/1538-4357/ab518b. URL: http://arxiv.org/abs/1910.12874 (visited on 05/14/2023).

[51] Nicholas Farrow, Xing-Jiang Zhu, and Eric Thrane. "The mass distribution of Galactic double neutron stars". In: *The Astrophysical Journal* 876.1 (Apr. 2019). arXiv:1902.03300 [astro-ph, physics:gr-qc], p. 18. ISSN: 1538-4357. DOI: 10.3847/1538-4357/ab12e3. URL: http://arxiv.org/abs/1902.03300 (visited on 05/14/2023).

[52] The LIGO Scientific Collaboration and the Virgo Collaboration. "GW190425: Observation of a Compact Binary Coalescence with Total Mass $\sim 3.4 M_{\odot}$". In: *The Astrophysical Journal Letters* 892.1 (Mar. 2020). arXiv:2001.01761 [astro-ph, physics:gr-qc], p. L3. ISSN: 2041-8205, 2041-8213. DOI: 10.3847/2041-8213/ab75f5. URL: http://arxiv.org/abs/2001.01761 (visited on 05/14/2023).

[53] Joaquim Iguaz, Pasquale D. Serpico, and Guillermo Franco-Abellán. "The QCD phase transition behind a PBH origin of LIGO/Virgo events?" en. In: *Journal of Cosmology and Astroparticle Physics* 2022.07 (July 2022). Publisher: IOP Publishing, p. 009. ISSN: 1475-7516. DOI: 10.1088/1475-7516/2022/07/009. URL: https://dx.doi.org/10.1088/1475-7516/2022/07/009 (visited on 05/14/2023).

[54] Christian T. Byrnes et al. "Primordial black holes with an accurate QCD equation of state". en. In: *Journal of Cosmology and Astroparticle Physics* 2018.08 (Aug. 2018), p. 041. ISSN: 1475-7516. DOI: 10.1088/1475-7516/2018/08/041. URL: https://dx.doi.org/10.1088/1475-7516/2018/08/041 (visited on 05/02/2023).

[55] Sebastien Clesse and Juan Garcia-Bellido. *GW190425, GW190521 and GW190814: Three candidate mergers of primordial black holes from the QCD epoch*. arXiv:2007.06481 [astro-ph, physics:gr-qc, physics:hep-ph]. May 2021. DOI: 10.48550/arXiv.2007.06481. URL: http://arxiv.org/abs/2007.06481 (visited on 05/02/2023).